

# DATA-DRIVEN PROBABILITY DENSITY FORECAST FOR STOCHASTIC DYNAMICAL SYSTEMS \*

MENG ZHAO<sup>†</sup> AND LIJIAN JIANG<sup>‡</sup>

**Abstract.** In this paper, a data-driven nonparametric approach is presented for forecasting the probability density evolution of stochastic dynamical systems. The method is based on stochastic Koopman operator and extended dynamic mode decomposition (EDMD). To approximate the finite-dimensional eigendecomposition of the stochastic Koopman operator, EDMD is applied to the training data set sampled from the stationary distribution of the underlying stochastic dynamical system. The family of the Koopman operators form a semigroup, which is generated by the infinitesimal generator of the stochastic dynamical system. A significant connection between the generator and Fokker-Planck operator provides a way to construct an orthonormal basis of a weighted Hilbert space. A spectral decomposition of the probability density function is accomplished in this weighted space. This approach is a data-driven method and used to predict the probability density evolution and real-time moment estimation. In the limit of the large number of snapshots and observables, the data-driven probability density approximation converges to the Galerkin projection of the semigroup solution of Fokker-Planck equation on a basis adapted to an invariant measure. The proposed method shares the similar idea to diffusion forecast, but renders more accurate probability density than the diffusion forecast does. A few numerical examples are presented to illustrate the performance of the data-driven probability density forecast.

**Key words.** Stochastic dynamical system, Stochastic Koopman operator, Probability density decomposition, Diffusion forecast

**1. Introduction.** Dynamical systems afford a mathematical framework to characterize the evolution of a physical process and model the abundant interactions between coupled physical quantities. Further, stochastic dynamical systems play a critical role in the analysis, prediction, and understanding of the behaviour of systems, or the flow maps that describe the evolution of stochastic processes. In this big data era, data are plentiful, while the governing equations or physical laws may be elusive in the practical scenarios such as the problems in climate science, finance and neuroscience. Inevitably, modern stochastic dynamical system is currently undergoing a renaissance, with analytical derivations complemented by data-driven modeling [5]. For the data-driven modeling in science and engineering, one of the fundamental problems is to discover high-dimensional dynamical systems from time-series data.

Transfer operator approach has drawn significant attention and been widely used for data-driven modeling in the past decades. In general, the transfer operator methods focus on the evolution of elements in observable spaces or measure spaces. These methods may approximate Koopman operator [8, 19, 22] and Perron-Frobenius operator [20, 29] by computing a finite-dimensional eigendecomposition of the operators. Remarkably, the action of Koopman operator on the observables lifts the action from the state space to the observable space through composition of the observable and the underlying dynamical flow map. The Koopman operator transforms the nonlinear, finite-dimensional dynamical system to a linear system in infinite dimensions. Therefore, the modeling of Koopman operator follows the linear operator theory and the finite-dimensional approximation will be utilized in practical computation.

---

\*L.Jiang acknowledges the support of NSFC 12271408 and the Fundamental Research Funds for the Central Universities.

<sup>†</sup>School of Mathematical Sciences, Tongji University, Shanghai 200092, China.  
(1910736@tongji.edu.cn).

<sup>‡</sup>School of Mathematical Sciences, Tongji University, Shanghai 200092, China.  
(ljjiang@tongji.edu.cn).

Data-driven mechanism of approximating the transfer operators has been widely investigated for a variety of applications, such as the identification of dynamical modes [8, 18, 20, 23], spectral analysis [1, 12, 24], nonparametric forecasting [2, 3, 15] and the modeling of slow-fast systems [9, 16]. The focus is on the estimation of the finite-dimensional projection of Koopman operator onto a specific subspace. This can be fulfilled by Dynamic Mode Decomposition(DMD) and its variants [10, 21, 31, 35, 36, 38, 39]. The DMD approach originates from computational fluid dynamics [32], and has been proven [30] that it gives the estimation of eigenvalues and modes of the Koopman operator under certain conditions. In what follows, we will use one of many varieties - Extended Dynamic Mode Decomposition(EDMD) algorithm, which is robust and works for stochastic dynamical systems [37], to approximate a finite-dimensional eigendecomposition of the Koopman operator. In EDMD, Koopman operator is projected to a finite-dimensional dictionary subspace of observables. Thus the eigenvalue problem becomes a matrix eigenvalue problem. In particular, the standard DMD (also known as exact DMD) is a specific case of EDMD for the dictionary space constituted by the state itself, which may not accurately characterize the action of Koopman operator. EDMD is able to give an accurate approximation to the Koopman operator when the dictionaries are elaborately selected. The choice of the dictionaries is very technical and critical. In the setting of ergodic dynamical systems, observable spaces are the nature  $L^2$  spaces of the scalar functions, and the measures are associated with  $L^2$  densities. Perron-Frobenius operator is the  $L^2$ -adjoint to Koopman operator. A common approach to approximate the Perron-Frobenius operator is celebrated as Ulam's method, and [20] has shown that Ulam's method and EDMD are dual each other.

For stochastic dynamical systems, the action of the Koopman operator takes the expectation of the composition of observable and flow map, and this Koopman operator is called stochastic Koopman operator [8]. The stochastic Koopman operator implies that the action of stochastic Koopman operator on observables represents the solution of the Backward Kolmogorov Equation (BKE) of the stochastic dynamical system with observables as initial condition. Furthermore, BKE is essentially governed by the infinitesimal generator of the stochastic dynamical system. Therefore, there is an elegant connection bewteen stochastic Koopman operator and the infinitesimal generator, i.e., the stochastic Koopman operator is an analytic and bounded semigroup generated by the infinitesimal generator of the stochastic dynamical system [26]. Under appropriate conditions, the infinitesimal generator is  $L^2$ -adjoint to Fokker-Planck operator. Besides, the Fokker-Planck operator characterizes the transitions of probabilities, which reveals that the Fokker-Planck operator is the generator of the corresponding Perron-Frobenius operator semigroup. It is worth noting that, for an ergodic and time-reversible stochastic dynamical system with a unique invariant measure, the infinitesimal generator is self-adjoint and non-positive in the weighted  $L^2$  space associated with the invariant measure. The self-adjointness and non-positivity guarantee that the eigenvalues of the generator are non-positive and real, and its spectrum are discrete in this specific Hilbert space. Thus the eigenfunctions of the generator constitute an orthonormal basis of weighted Hilbert space. Moreover, eigenvalues can be sorted by magnitude to extract the slow behaviours, which correspond to larger eigenvalues. The fast behaviours describe noise. The above mentioned relationship motivates us to estimate the eigendecomposition of the Fokker-Planck operator through the data-driven method, and approximate the probability density functions in the space spanned by the eigenfunctions.

In this paper, given a set of time-series data, our target is to approximate the probability density function of the stochastic dynamical systems. We adapt EDMD method to a weighted  $L^2$  space to obtain the approximation of the Koopman operator. Hence the eigendecomposition of the infinitesimal generator can be computed through the relationship between the generator and semigroup. Then the adjoint property between the infinitesimal generator and Fokker-Planck operator provides a way to procure the eigenpairs of Fokker-Planck operator. Finally, we decompose the probability density function in the space spanned by the eigenfunctions of the Fokker-Planck operator, and use the Fokker-Planck equation to analytically compute the coefficient functions evolved in time. We call the proposed method as dynamic probability density decomposition (DPDD). The approach allows that the time-series data can be not only from one single long-time trajectory, but also from ensemble trajectories. But, the utilization of EDMD requires that the data must be data pairs. As a similar method, the diffusion forecast method proposed in [2, 3] is also to estimate the probability density function using the eigenfunctions of the generator of a specific gradient flow system. It utilizes the diffusion maps [6, 7] to approximate the eigenfunctions. Comparing to diffusion forecast, our approach analytically compute the time-dependent coefficients of the decomposition without approximation error, which occurs in diffusion forecast. Our analysis and numerical results show that DPDD achieves better accuracy and efficiency than the diffusion forecast.

The paper is organized as follows. In Section 2, we briefly introduce the infinitesimal generator, Fokker-Planck operator, Backward Kolmogorov equation and stochastic Koopman operator for stochastic dynamical systems. Dynamic probability density decomposition is elaborated in Section 3. Besides, we also review the diffusion forecast method and make a comparison between diffusion forecast and the Koopman operator-based DPDD. The convergence of DPDD is analyzed in Section 4. A few numerical results are presented to illustrate the probability density forecast using DPDD in Section 5. Some conclusions and comments are made in Section 6.

**2. Preliminaries.** In this section, we give a short review on stochastic dynamical systems and their infinitesimal generator, and present the connection with Koopman operator and its generator. These will be used in the whole paper.

**2.1. The infinitesimal generator of SDE and its adjoint operator.** Consider a time-homogeneous Markov process  $X_t \in \mathcal{M} \subseteq \mathbb{R}^d$ , which is generated by the SDE with drift term  $b(x) : \mathbb{R}^d \rightarrow \mathbb{R}^d$ , diffusion function  $\sigma(x) : \mathbb{R}^d \rightarrow \mathbb{R}^{d \times s}$ , and  $s$ -dimensional Wiener process  $W_t$ , i.e., the  $X_t$  solves the autonomous dynamical system,

$$dX_t = b(X_t)dt + \sigma(X_t)dW_t, \quad X(0) = X_0. \quad (2.1)$$

The (infinitesimal) generator  $\mathcal{L}$  of SDE (2.1) is then defined by

$$\mathcal{L}v = b \cdot \nabla v + \frac{1}{2}\Sigma : \nabla \nabla v, \quad (2.2)$$

where  $\Sigma(x) = \sigma(x)\sigma^T(x)$  is the diffusion matrix. The formal  $L^2$ -adjoint operator  $\mathcal{L}^*$  (a.k.a., the Fokker-Planck operator) is defined by

$$\mathcal{L}^*v = -\nabla \cdot (bv) + \frac{1}{2}\nabla \cdot \nabla \cdot (\Sigma v). \quad (2.3)$$

**THEOREM 2.1.** [25, 28] (**Backward Kolmogorov Equation**) *Let  $f : \mathcal{M} \rightarrow \mathbb{R}$  and define*

$$v(x, t) = \mathbb{E}(f(X_t) | X(0) = x),$$

where the expectation is with respect to the Wiener process. If  $f$  is smooth, then the following equation

$$\begin{cases} \frac{\partial v}{\partial t} = \mathcal{L}v, & (x, t) \in \mathcal{M} \times (0, \infty), \\ v(x, 0) = f(x), \end{cases} \quad (2.4)$$

has a unique bounded classical solution  $v(x, t) \in \mathcal{C}^{2,1}(\mathcal{M} \times \mathbb{R}^+)$ .

We assume that the initial state  $X_0$  is a random variable with probability density function  $p_0(x)$ , and the transition probability density function  $p(x, t)$  exists and is a function in  $\mathcal{C}^{2,1}(\mathcal{M} \times \mathbb{R}^+)$ . Then  $p(x, t)$  satisfies the **Fokker-Planck equation** [27, 28, 34] (a.k.a., the **forward Kolmogorov equation**),

$$\begin{cases} \frac{\partial p(x, t)}{\partial t} = \mathcal{L}^* p(x, t), & (x, t) \in \mathcal{M} \times (0, \infty), \\ p(x, 0) = p_0(x). \end{cases} \quad (2.5)$$

Let the probability flux

$$J(x, t) := b(x)p(x, t) - \frac{1}{2}\nabla \cdot (\Sigma(x)p(x, t)). \quad (2.6)$$

Then the Fokker-Planck equation can be written as

$$\frac{\partial p(x, t)}{\partial t} + \nabla \cdot J = 0.$$

Under periodic boundary condition and the assumption on the uniformly positive definition of diffusion matrix  $\Sigma(x)$  [27], the stochastic process  $X_t$  is ergodic. Then the unique invariant distribution  $p_s(x)$  exists and solves

$$\nabla \cdot J_s := \nabla \cdot (b(x)p_s(x)) - \frac{1}{2}\nabla \cdot \nabla \cdot (\Sigma(x)p_s(x)) = 0. \quad (2.7)$$

This implies the equilibrium probability flux is a divergence-free vector field. If we consider a reflecting boundary condition in a bounded domain for Fokker-Planck equation (2.5), then the stationary flux vanishes  $J_s(x) = 0$ . This is a stronger condition than (2.7), since it involves  $d$  equations, whereas the divergence-free equation (2.7) is only one equation. Thus, in general, the stationary probability flux does not vanish. If the stochastic process  $X_t$  satisfies the detailed balance equation,

$$p_s(x)p(y, t|x, s) = p_s(y)p(x, t|y, s), \quad \forall x, y \in \mathcal{M}, s < t, \quad (2.8)$$

then the stationary probability flux is zero. Therefore, for a time-reversible process, the probability flux vanishes in steady state. In what follows, we will assume the time-homogeneous process  $X_t$  is reversible. Conditions on the coefficients  $b(x)$  and  $\Sigma(x)$  that are both necessary and sufficient for the detailed balance to be satisfied can be founded in [13, 14], and this paper will do not discuss it further.

**REMARK 2.1.** *The fact that the solution of Fokker-Planck equation is a probability density means that*

$$\int_{\mathcal{M}} p(x, t)dx = 1, \quad p(x, t) \geq 0 \quad \forall t \in \mathbb{R}^+,$$

and

$$\int_{\mathcal{M}} p_s(x) dx = 1, \quad p_s(x) \geq 0.$$

Next, our objective is to establish the connection between Koopman operator and the infinitesimal generator. To accomplish this, we recall Koopman operator in Subsection 2.2.

**2.2. Koopman operator.** For a continuous-time deterministic system [8, 20] defined on measure space  $(\mathcal{M}, \mathfrak{B}, \nu)$ ,

$$\begin{cases} \dot{x} = \mathbf{F}(x), & x \in \mathcal{M}, \\ x(0) = x_0, \end{cases}$$

where  $\mathcal{M} \subseteq \mathbb{R}^d$  is the state space,  $\mathfrak{B}$  is a sigma-algebra, and  $\nu$  is a measure. The flow map (or evolution operator) is  $\phi^t(x_0) := x(t, x_0)$ . Koopman operator  $\mathcal{K}^t$  acts on the real-valued observable of the state space,  $\psi : \mathcal{M} \rightarrow \mathbb{R}$ , and we define the Koopman operator by

$$\mathcal{K}^t \psi(x) = \psi \circ \phi^t(x) = \psi(\phi^t(x)), \quad (2.9)$$

where  $\circ$  denotes the function composition. If the observable  $\varphi : \mathcal{M} \rightarrow \mathbb{R}$  and satisfies

$$\mathcal{K}^t \varphi(x) = \mu(t) \varphi(x), \quad (2.10)$$

then  $\varphi(x)$  is an eigenfunctions of the Koopman operator and the corresponding  $\mu(t)$  is the eigenvalue. The Koopman operator  $\mathcal{K}^t$  is an infinite-dimensional linear operator and describes the evolution of observables, and lifts the finite-dimensional nonlinear dynamical system  $\phi^t$  to a linear system in infinite dimensions.

For a continuous-time random dynamical system (RDS)  $(\mathcal{M}, \mathcal{F}, P, \Phi^t)$  [8], the stochastic Koopman operator is defined as

$$\mathcal{K}^t \psi(x) = \mathbb{E}[\psi \circ \Phi^t(x)] = \mathbb{E}[\psi(\Phi^t(x))], \quad (2.11)$$

where  $\mathbb{E}[\cdot]$  is the expectation value with respect to the probability measure  $P$ . For autonomous SDE (2.1), the flow map  $\Phi^t(x)$  in (2.11) is defined as

$$\Phi^t(x) := x + \int_0^t b(X_s) ds + \sigma(X_s) dW_s := X_t^x.$$

The Koopman operators mentioned previously are assumed to be time-homogeneous Markovian. For inhomogeneous time-varying random dynamical system  $(\mathcal{M}, \mathcal{F}, P, \tilde{\Phi}^{t,t_0})$ , the Koopman operator is defined by a two-parameter family of operator:  $\mathcal{K}^{t,t_0} \psi(x) = \mathbb{E}[\psi(\tilde{\Phi}^{t,t_0}(x))]$ . We remark the difference between the definitions of two kinds of Koopman operators. For time-homogeneous system, the Koopman operator is associated with the flow map  $\Phi^{\Delta t}$  only dependent on the time interval  $\Delta t$ , while the Koopman operator of time-varying system is determined by a two-parameter flow map  $\tilde{\Phi}^{t,t_0}$  depending on both the current time  $t$  and the initial time  $t_0$ . Since we focus on the autonomous stochastic dynamical systems in this work, the one-parameter Koopman operator family is only considered herein.

Combining the backward Kolmogorov equation (2.4) and the definition (2.11) of Koopman operator, we have the following relation between the Koopman operator and infinitesimal generator of SDE,

$$\mathcal{L}\psi = \mathcal{L}_K\psi := \lim_{t \rightarrow 0^+} \frac{\mathcal{K}^t\psi - \psi}{t}, \quad \forall \psi \in \mathcal{F}, \quad (2.12)$$

where  $\mathcal{L}_K$  is the generator that generates the Koopman semigroup. (2.12) implies that the infinitesimal generator of SDE is exactly the generator of Koopman operator. Thus we will do not distinguish them, and denote them by  $\mathcal{L}$  from now on. We note that the spectrum of generator  $\mathcal{L}$  on a specific weighted Hilbert space defined in Section 3 is discrete, and lies along the negative real axis and tends to  $-\infty$ . The infinitesimal generator  $\mathcal{L}$  is sectorial and the semigroup  $\mathcal{K}$  generated by  $\mathcal{L}$  is analytic and bounded. Given  $e^{0\mathcal{L}} = I$ , the following properties hold.

PROPOSITION 2.2. [26]

- (i) For  $\forall s, t \geq 0$ ,  $e^{s\mathcal{L}}e^{t\mathcal{L}} = e^{(s+t)\mathcal{L}}$ ;
- (ii) For  $\forall t \geq 0$ , and every  $k \in \mathbb{N}$ ,  $\mathcal{L}^k e^{t\mathcal{L}} = e^{t\mathcal{L}}\mathcal{L}^k$ ;
- (iii) For  $\forall t > 0$ ,  $\frac{d^k}{dt^k}e^{t\mathcal{L}} = \mathcal{L}^k e^{t\mathcal{L}}$ .

This indicates that there is a neat connection between the eigenpairs of Koopman operator  $\mathcal{K}^t = e^{t\mathcal{L}}$  and generator  $\mathcal{L}$ ,

$$\mathcal{K}^t\varphi(x) = \mu(t)\varphi(x) = e^{t\mathcal{L}}\varphi(x) = e^{t\lambda}\varphi(x), \quad (2.13)$$

where  $(\lambda, \varphi)$  are the eigenpairs of generator  $\mathcal{L}$ . Thus once we have the approximation of eigenpairs of Koopman operator, the eigendecomposition of generator  $\mathcal{L}$  is available.

**3. Dynamic Probability Density Decomposition.** Assume that (2.8) is satisfied as we discussed in Subsection 2.1, then we have the vanished stationary probability flux and obtain the equality

$$b(x)p_s(x) = \frac{1}{2}\nabla \cdot (\Sigma(x)p_s(x)). \quad (3.1)$$

Consider a set of functions  $p(x, t) \in \mathfrak{D}(\mathcal{L}^*)$ , and next we derive a connection between the action of the infinitesimal generator on observables and the action of Fokker-Planck operator on distributions. This is a generalization of the relation for gradient flows presented in [17].

PROPOSITION 3.1. *Let  $p(x, t) = f(x, t)p_s(x)$ . Then the following holds,*

$$\mathcal{L}^*p = p_s\mathcal{L}f. \quad (3.2)$$

*Proof.* By the definition of Fokker-Planck operator, we have

$$\begin{aligned}
\mathcal{L}^* p &= \nabla \cdot (-b(x)p(x, t)) + \frac{1}{2}\nabla \cdot \nabla \cdot (\Sigma(x)p(x, t)) \\
&= \nabla \cdot (-b(x)f(x, t)p_s(x)) + \frac{1}{2}\nabla \cdot \nabla \cdot (\Sigma(x)f(x, t)p_s(x)) \\
&= -b(x)p_s(x)\nabla f - f\nabla \cdot (b(x)p_s(x)) \\
&\quad + \frac{1}{2}\nabla \cdot (\Sigma(x)p_s(x)\nabla f + f\nabla \cdot (\Sigma(x)p_s(x))) \\
&= -b(x)p_s(x)\nabla f + \frac{1}{2}\Sigma(x)p_s(x) : \nabla \nabla f + \nabla f \nabla \cdot (\Sigma(x)p_s(x)) \\
&\quad - f\left(\nabla \cdot [b(x)p_s(x) - \frac{1}{2}\nabla \cdot (\Sigma(x)p_s(x))]\right) \\
&= \frac{1}{2}\Sigma(x)p_s(x) : \nabla \nabla f + b(x)p_s(x)f \\
&= p_s \mathcal{L} f,
\end{aligned}$$

where the equality (3.1) is used in the third step.  $\square$

Besides, we also have  $\mathcal{L} f = p_s^{-1} \mathcal{L}^* p = p_s^{-1} \mathcal{L}^*(f p_s) = p_s^{-1} \frac{\partial(f p_s)}{\partial t} = \frac{\partial f}{\partial t}$ . This shows that  $f(x, t)$  satisfies the backward Kolmogorov equation.

In what follows we consider the weighted Hilbert  $L^2$ -space  $L^2(\mathcal{M}; p_s)$  weighted by the stationary distribution  $p_s(x)$  with norm

$$\|f\|_{0, p_s}^2 = \langle f, f \rangle_{p_s} = \int_{\mathcal{M}} |f|^2 p_s(x) dx. \quad (3.3)$$

We claim that the generator  $\mathcal{L}$  is self-adjoint and  $-\mathcal{L}$  is positive and semi-definite with respect to  $L^2(\mathcal{M}; p_s)$ . The self-adjointness can be verified by noting that, for any pair of functions  $f, g \in L^2(\mathcal{M}; p_s)$ ,

$$\langle \mathcal{L} f, g \rangle_{p_s} = \langle \mathcal{L} f, g p_s \rangle = \langle f, \mathcal{L}^*(g p_s) \rangle = \langle f, p_s \mathcal{L} g \rangle = \langle f, \mathcal{L} g \rangle_{p_s},$$

where we have utilized the fact (3.2) in the third equality. The positiveness and semi-definite can be obtained by noting that for any function  $f \in L^2(\mathcal{M}; p_s)$ ,

$$\begin{aligned}
\langle -\mathcal{L} f, f \rangle_{p_s} &= \langle -\mathcal{L} f, f p_s \rangle \\
&= -\langle b(x) \cdot \nabla f + \frac{1}{2}\Sigma : \nabla \nabla f, f p_s \rangle \\
&= -\frac{1}{2}\langle \nabla \cdot (\Sigma p_s) \nabla f, f \rangle - \langle \frac{1}{2}\Sigma : \nabla \nabla f, f p_s \rangle \\
&= \frac{1}{2}\langle \Sigma \nabla f, \nabla f \rangle_{p_s} \\
&= \frac{1}{2}\|\sigma^T \nabla f\|_{p_s} \geq 0.
\end{aligned}$$

We assume that the generator  $\mathcal{L}$  has a set of discrete spectrum. Then the eigenfunctions  $\{\varphi_j\}_{j=1}^\infty$  form an orthonormal basis of  $L^2(\mathcal{M}; p_s)$ . Therefore, for any observable  $f \in L^2(\mathcal{M}; p_s)$ , the spectral expression  $f(x, t) = \sum_j f_j(t) \varphi_j(x)$  with  $f_j(t) = \langle f, \varphi_j \rangle$  holds. Recall the equality (3.2)  $\mathcal{L}^* p = p_s \mathcal{L} f$ , which immediately indicates that  $\mathcal{L}^*(\varphi_j p_s) = p_s \mathcal{L} \varphi_j = p_s \lambda_j \varphi_j = \lambda_j \varphi_j p_s$ . Thus,  $\{\varphi_j p_s\}_{j=1}^\infty$  are the eigenfunctions of the Fokker-Planck operator  $\mathcal{L}^*$  with respect to eigenvalues  $\{\lambda_j\}_{j=1}^\infty$ . Moreover, the

eigenfunctions of  $\mathcal{L}^*$  form an orthonormal basis of space  $L^2(\mathcal{M}; p_s^{-1})$  following the orthonormality of  $\{\varphi_j\}_{j=1}^\infty$ ,

$$\langle \varphi_i p_s, \varphi_j p_s \rangle_{p_s^{-1}} = \langle \varphi_i, \varphi_j \rangle_{p_s} = \delta_{ij}.$$

**3.1. The spectral expansion.** Given an orthonormal basis of  $L^2(\mathcal{M}; p_s^{-1})$ , we can express the solution of the Fokker-Planck equation in (2.5) in the following form,

$$p(x, t) = e^{t\mathcal{L}^*} p_0(x) = \sum_{i=0}^{\infty} c_i(t) \varphi_i(x) p_s(x). \quad (3.4)$$

In order to obtain the system for the coefficients  $c_i(t)$ , we substitute (3.4) into the Fokker-Planck equation (2.5) and utilize the Galerkin method, we have an ODE system for the coefficients  $c_i(t)$ ,  $\forall i = 0, 1, \dots, \infty$ ,

$$\begin{aligned} c_i(t) &= \langle e^{t\mathcal{L}^*} p_0(x), \varphi_i(x) p_s(x) \rangle_{p_s^{-1}} \\ &= \langle p_0(x), e^{t\mathcal{L}} \varphi_i(x) \rangle \\ &= \left\langle \sum_{j=0}^{\infty} c_j(0) \varphi_j(x) p_s(x), e^{t\mathcal{L}} \varphi_i(x) \right\rangle \\ &= \sum_{j=0}^{\infty} c_j(0) \langle \varphi_j(x), e^{\lambda_i t} \varphi_i(x) \rangle_{p_s} \\ &= \sum_{j=0}^{\infty} e^{\lambda_i t} \delta_{ij} c_j(0) \\ &= e^{\lambda_i t} c_i(0). \end{aligned} \quad (3.5)$$

Here the eigenpair  $(\lambda_i, \varphi_i)$  are the eigenvalues and eigenfunctions of the generator  $\mathcal{L}$ , and  $c_i(0)$  are the coordinates of the initial condition  $p_0(x)$  under the basis of eigenfunctions  $\{\varphi_i p_s\}_{i=1}^\infty$ . Thus combining (3.4) and (3.5) we can represent the probability density function  $p(x, t)$  as follows,

$$p(x, t) = \sum_{i=0}^{\infty} e^{\lambda_i t} \varphi_i(x) p_s(x) c_i(0), \quad (3.6)$$

where  $c_i(0) = \langle p_0(x), \varphi_i p_s \rangle_{p_s^{-1}}$ .

By the spectral expansion (3.6), we can obtain the probability density function without knowing the dynamical system (2.1) and the manifold  $\mathcal{M}$ . In fact, all we need is that the eigendecomposition of the generator  $\mathcal{L}$ , which can be obtained by EDMD described in Subsection 3.2.2. Next, the data-driven method (EDMD) is going to be introduced for the numerical approximation of the spectral expansion.

**3.2. Data-driven approximation.** In this subsection, we briefly recall the extended dynamic mode decomposition (EDMD) for deterministic systems, and apply it to the stochastic dynamical systems with ergodicity.

**3.2.1. Extended Dynamic mode decomposition.** In this subsection, we elaborate EDMD [21, 37], which is a data-driven method to approximate the Koopman operator. Assume that we are given a data set of snapshots pairs  $\{(x_m, y_m)\}_{m=1}^M$ ,

$$\mathbf{X} = [x_1, x_2, \dots, x_M], \quad \mathbf{Y} = [y_1, y_2, \dots, y_M]$$

satisfying  $y_m = \Phi^{\Delta t}(x_m)$ , where  $\Delta t$  is the temporal interval of snapshots. Typically, the data samples are not necessarily required to lie on a single trajectory. EDMD requires that a dictionary of observables,  $\mathcal{D} = \{\psi_1, \psi_2, \dots, \psi_N \mid \psi_i \in \mathcal{F}\}$ , whose span is denoted as  $\mathcal{F}_{\mathcal{D}} \subset \mathcal{F}$ . For brevity, we define the vector-valued observable  $\psi : \mathcal{M} \rightarrow \mathbb{R}^{1 \times N}$ , where  $\psi(x) = [\psi_1(x), \psi_2(x), \dots, \psi_N(x)]^T$ . EDMD constructs a finite-dimensional approximation  $\mathbf{K} \in \mathbb{R}^{N \times N}$  of Koopman operator by solving the least-squares problem,

$$\min_{\mathbf{K} \in \mathbb{R}^{N \times N}} \|\mathbf{K}\psi(\mathbf{X}) - \psi(\mathbf{Y})\|_F^2 = \min_{\mathbf{K} \in \mathbb{R}^{N \times N}} \sum_{m=1}^M \|\mathbf{K}\psi(x_m) - \psi(y_m)\|_2^2, \quad (3.7)$$

where  $\psi(\mathbf{X}) = [\psi(x_1), \dots, \psi(x_M)]$ ,  $\psi(\mathbf{Y}) = [\psi(y_1), \dots, \psi(y_M)]$ . The  $\mathbf{K}$  minimizes (3.7) is

$$\mathbf{K} = \psi(\mathbf{Y})\psi(\mathbf{X})^\dagger,$$

where  $\dagger$  denotes the pseudoinverse. This approach will require expensive computation for large  $M$ , since it needs the pseudoinverse of the  $N \times M$  matrix  $\psi(\mathbf{X})$ . Thus one usually takes another approach to compute  $\mathbf{K}$ ,

$$\mathbf{K} = AG^\dagger, \quad (3.8)$$

where the relationship  $\psi(\mathbf{X})^\dagger = \psi(\mathbf{X})^T (\psi(\mathbf{X})\psi(\mathbf{X})^T)^{-1}$  is utilized and

$$\begin{aligned} G &= \frac{1}{M} \sum_{m=1}^M \psi(x_m)\psi(x_m)^T, \\ A &= \frac{1}{M} \sum_{m=1}^M \psi(y_m)\psi(x_m)^T. \end{aligned} \quad (3.9)$$

As a result, we have  $\mathbf{K}$  as a finite-dimensional approximation of  $\mathcal{K}$ . Thus, if  $\xi_i \in \mathbb{R}^{N \times 1}$  is the  $i$ -th left eigenvector of  $\mathbf{K}$  with the associated eigenvalue  $\mu_i$ , then the EDMD approximation of an eigenfunction of  $\mathcal{K}$  is given by

$$\phi_i(x) = \xi_i^T \psi(x).$$

**3.2.2. EDMD in weighted Hilbert space.** Although EDMD was proposed for the deterministic systems and the deterministic Koopman operator in the beginning, it can also be applied to data from stochastic systems without changing the procedure. As shown in Subsection 3.2.1, EDMD can give the eigenpair  $(\mu_i, \varphi_i)$  of Koopman operator  $\mathcal{K}$ , whose eigenfunctions are also the eigenfunctions of the generator  $\mathcal{L}$  with respect to the eigenvalues  $\lambda_i = \frac{\log \mu_i}{\Delta t}$  in Hilbert space  $L^2(\mathcal{M})$ . But we actually need the eigenpairs in the weighted Hilbert space  $L^2(\mathcal{M}; p_s)$ , we modify EDMD to adapt to this situation. The data set  $\{x_i\}_{i=0}^M$  is sampling from stationary density function  $p_s$ , and EDMD will employ these data to approximate the eigendecomposition in weighted space. In this weighted Hilbert space, for  $\forall f, g \in L^2(\mathcal{M}; p_s)$ , we have an estimation for the inner product of two observables by these stationary data,

$$\langle f, g \rangle_{p_s} \approx \frac{1}{M} \sum_{i=0}^M f(x_i)g(x_i).$$

To obtain the eigenpairs of generator  $\mathcal{L}$ , we utilize the data observed at those sample points, i.e., the snapshot matrix is as follows,

$$(\psi(x_0), \psi(x_1), \dots, \psi(x_M)) = \begin{pmatrix} \psi_1(x_0) & \psi_1(x_1) & \dots & \psi_1(x_M) \\ \psi_2(x_0) & \psi_2(x_1) & \dots & \psi_2(x_M) \\ \vdots & \vdots & \ddots & \vdots \\ \psi_N(x_0) & \psi_N(x_1) & \dots & \psi_N(x_M) \end{pmatrix}, \quad (3.10)$$

where  $\psi = (\psi_1, \psi_2, \dots, \psi_N)^T$  is the vector-valued observation function. Given

$$\begin{aligned} \psi(X) &= \begin{pmatrix} \psi_1(x_0) & \psi_1(x_1) & \dots & \psi_1(x_M) \\ \psi_2(x_0) & \psi_2(x_1) & \dots & \psi_2(x_M) \\ \vdots & \vdots & \ddots & \vdots \\ \psi_N(x_0) & \psi_N(x_1) & \dots & \psi_N(x_M) \end{pmatrix}, \\ \psi(Y) &= \begin{pmatrix} \psi_1(y_0) & \psi_1(y_1) & \dots & \psi_1(y_M) \\ \psi_2(y_0) & \psi_2(y_1) & \dots & \psi_2(y_M) \\ \vdots & \vdots & \ddots & \vdots \\ \psi_N(y_0) & \psi_N(y_1) & \dots & \psi_N(y_M) \end{pmatrix}, \end{aligned} \quad (3.11)$$

where  $y_i = \Phi^{\Delta t}(x_i)$ ,  $\Phi$  is the evolution operator associated with the stochastic dynamical system. We can get the approximation of  $\Phi$  by using Euler-Maruyama method, Milstein scheme, etc.. We apply the standard EDMD method in Subsection 3.2.1 to above snapshot matrixs (3.11) and get the eigendecomposition in weighted space. Ultimately, we obtain the approximate dynamic probability density decomposition,

$$p_N(x, t) = \sum_{i=1}^N e^{\lambda_i t} \varphi_i(x) p_s(x) \tilde{c}_i(0), \quad (3.12)$$

where  $\tilde{c}_i(0)$  is an Monte-Carlo approximation of coefficients  $c_i(0) = \langle p_0(x), \varphi_i p_s \rangle_{p_s^{-1}} = \mathbb{E}^0(\varphi_i)$  in the dynamic probability density decomposition (3.6).  $(\lambda_i, \varphi_i)$  is the eigenpairs of generator  $\mathcal{L}$ , which is associated with the eigenpairs  $(\mu_i, \varphi_i)$ , acquired by EDMD, of Koopman operator.

If we compute  $c_i(0)$  by standard Monte-Carlo integration method, we may need the abundant independent samples drawn from the initial distribution  $p_0(x)$ . This is computationally expensive and the initial distribution may be hard to sample. To address this intractable problem, we use the snapshots data  $\{x_i\}_{i=0}^M$  sampled from stationary distribution to approximate the expectation by means of the importance sampling approach. The alternative distribution is the stationary distribution, which is needed to be absolutely continuous with respect to the initial distribution  $p_0(x)$ . Then the importance sampling estimator of  $c_i(0)$  is given by

$$\tilde{c}_i(0) = \frac{1}{M+1} \sum_{i=0}^M \varphi_i(x_i) p_0(x_i) / p_s(x_i).$$

In this way, the variance of estimator will be zero when the stationary density is exactly equal to  $p_0(x) \varphi_i(x) / c_i(0)$ . Nevertheless, we can not really reach this zero-variance, since we do not know the accurate value of  $c_i(0)$ . If the stationary distribution  $p_s(x)$  is proportional to the product of the initial density  $p_0(x)$  and the basis function  $\varphi_i(x)$ ,

**Algorithm 1** Dynamic Probability Density decomposition(DPDD)

---

**Input:** Data set of snapshots pairs  $\{(x_i, y_i)\}_{i=0}^M$  sampling from invariant density  $p_s(x)$ , such that  $y_i = \Phi^{\Delta t}(x_i)$ ; the initial condition  $p_0(x)$ .

**Output:** The probability density function  $p(x, t)$  and the eigenpairs  $\{(\lambda_i, \varphi_i)\}$  of the infinitesimal generator  $\mathcal{L}$ .

**1:** Choose the appropriate observational space  $\mathcal{F}_D = \text{span}\{\psi_1, \psi_2, \dots, \psi_N\}$ , and generate the snapshots matrices  $\psi(X)$ ,  $\psi(Y)$  given in (3.11).

**2:** Compute the Koopman matrix using formula (3.8) and (3.9), then the eigenpairs  $\{(\mu_i, \varphi_i)\}$  can be obtained by the eigendecomposition of Koopman matrix. And the eigenpairs  $\{(\lambda_i, \varphi_i)\}$  of the infinitesimal generator  $\mathcal{L}$  can be computed by the use of the relationship (2.13).

**3:** Approximate the probability density function  $p(x, t)$  by equation (3.6), with coefficients  $\tilde{c}_i(0) = \frac{1}{M+1} \sum_{i=0}^M p_0(x_i) \varphi_i(x_i) / p_s(x_i)$ .

---

the variance can be significantly reduced. In the end, we summarize our approach in Algorithm 1.

**3.3. Diffusion forecast.** As another nonparametric forecasting method, diffusion forecast (DF) [2, 3, 17] shares the similar idea to the proposed dynamic probability density decomposition, and treated stochastic gradient systems with isotropic diffusion coefficient at the beginning. In the diffusion forecast, diffusion map is a key technique to acquire the approximate eigendecomposition of an operator, which is the infinitesimal generator of a stochastic gradient flow with the invariant density function of system state as the potential energy. Then diffusion forecast uses the eigenfunctions of this specified generator as the basis to estimate the probability density function with a finite-dimensional truncation. In this subsection, we present the diffusion forecast and explore the relation between the diffusion forecast and the probability density forecast of Koopman operator.

For the diffusion forecast method, we consider the same dynamical system as (2.1). DF assumes that the system is ergodic with the unique equilibrium density  $p_s(x)$  and given a time series data  $x_i := x(t_i) \sim p_s(x)$ . The goal of DF is to approximate  $p(x, t)$  utilizing the given data without knowing the model. DF proposes using the diffusion maps algorithm to estimate the generator  $\hat{\mathcal{L}} = \nabla \log(p_s) \cdot \nabla + \Delta$  of gradient flow,

$$dx = \nabla \log(p_s(x)) dt + \sqrt{2} dW_t. \quad (3.13)$$

The gradient flow system has the exactly same stationary distribution as the underlying system (2.1). As a particular case of generator,  $\hat{\mathcal{L}}$  is naturally self-adjoint and non-positive with respect to the weighted space  $L^2(\mathcal{M}; p_s)$  as we have previously discussed in this section. By the diffusion map algorithm, DF estimates the eigenpairs  $(\hat{\lambda}_i, \hat{\varphi}_i)$  of generator  $\hat{\mathcal{L}}$ , rather than those of generator  $\mathcal{L}$  of underlying system (2.1). Then the density function in DF is expressed as the following form,

$$p(x, t) = \sum_{k=0}^{\infty} \hat{c}_k(t) \hat{\varphi}_k(x) p_s(x), \quad (3.14)$$

where the coefficients  $\hat{c}_k(t)$  can be computed as follows,

$$\begin{aligned}
\hat{c}_k(t) &= \langle e^{t\mathcal{L}^*} p_0, \hat{\varphi}_k p_s \rangle_{p_s}^{-1} \\
&= \langle p_0, e^{t\mathcal{L}} \hat{\varphi}_k \rangle \\
&= \langle \sum_{j=0}^{\infty} \hat{c}_j(0) \hat{\varphi}_j p_s, e^{t\mathcal{L}} \hat{\varphi}_k \rangle \\
&= \sum_{j=0}^{\infty} \langle \hat{\varphi}_j, e^{t\mathcal{L}} \hat{\varphi}_k \rangle_{p_s} \hat{c}_j(0).
\end{aligned} \tag{3.15}$$

In practical computation, DF also truncates the summation with a finite terms, and produces a matrix-vector multiplication,  $\tilde{c}(t) = B\tilde{c}(0)$ , with  $k$ -th component  $\hat{c}_k(t)$ . And the  $kj$ -th entry of the matrix  $B$  is  $B_{kj} = \langle \hat{\varphi}_j, e^{t\mathcal{L}} \hat{\varphi}_k \rangle_{p_s}$ . Since the operator  $\hat{\mathcal{L}}$  is the generator relevant to the gradient flow rather than the underlying system (2.1), DF needs to approximate the coefficient matrix  $B$ . But our approach can compute the coefficients analytically and explicitly by using the generator  $\mathcal{L}$  of underlying system (2.1). In DF method, the components of  $B$  is numerically estimated as

$$B_{kj} = \langle \hat{\varphi}_j, e^{t\mathcal{L}} \hat{\varphi}_k \rangle_{p_s} \approx \langle \hat{\varphi}_j, S_t \hat{\varphi}_k \rangle_{p_s} \approx \frac{1}{M-1} \sum_{i=1}^{M-1} \hat{\varphi}_j(x_i) \hat{\varphi}_k(x_{i+1}), \tag{3.16}$$

where  $S_t$  is a shift operator such that  $S_t \hat{\varphi}_k(x_i) = \hat{\varphi}_k(x_{i+1})$ . We discover that

$$B_{kj} = \langle \hat{\varphi}_j, e^{t\mathcal{L}} \hat{\varphi}_k \rangle_{p_s} = \langle \hat{\varphi}_j, \mathcal{K}^t \hat{\varphi}_k \rangle_{p_s} = \langle \hat{\varphi}_j, \mathbb{E}(\hat{\varphi}_k \circ \Phi^t(x)) \rangle_{p_s}.$$

Therefore the shift operator  $S_t$  actually follows the action criteria of deterministic Koopman operator, and is used as an approximation of the stochastic Koopman operator in diffusion forecast method.

REMARK 3.1. *If the underlying system (2.1) is a gradient flow with the isotropic diffusion,*

$$dx = -\nabla V dx + \sqrt{2/\beta} dW_t,$$

*then DF has a trivial model with an analytic expression for the coefficient matrix  $B$ . In this special case, the underlying system (2.1) is exactly same as the gradient system (3.13) with the generator  $\hat{\mathcal{L}}$ . We can derive that the stationary Gibbs distribution  $p_s = \frac{1}{Z} \exp(-\beta V(x))$  is a solution of time-homogeneous Fokker-Planck equation, where  $Z = \int_{\mathcal{M}} e^{-\beta V(x)} dx$  is the normalization constant,*

$$\begin{aligned}
p_s &= \frac{1}{Z} \exp(-\beta V(x)) \\
\Rightarrow \frac{\nabla p_s}{p_s} &= \frac{\nabla(e^{-\beta V})}{e^{-\beta V}} = \nabla \log(e^{-\beta V}) = -\beta \nabla V \\
\Rightarrow \nabla p_s &= -\beta \nabla V \cdot p_s \\
\Rightarrow \mathcal{L}^* p_s &= \nabla \cdot (\beta \nabla V \cdot p_s) + \Delta p_s = 0.
\end{aligned}$$

*For the sake of simplicity, we assume that the normalization constant  $Z = 1$  and  $\beta = 1$ . Thus*

$$\hat{\mathcal{L}} = \nabla \log(p_s) \cdot \nabla + \Delta = \nabla \log(\exp(-V)) \cdot \nabla + \Delta,$$

and the generator of underlying system (2.1),  $\mathcal{L} = -\nabla V \cdot \nabla + \Delta$ . Consequently,  $\mathcal{L} = \hat{\mathcal{L}}$ , which can be estimated by the diffusion map algorithm. Let  $\mathcal{L}\hat{\varphi}_i = \hat{\lambda}_i\hat{\varphi}_i$ . In this case, DF can achieve the matrix  $B$  analytically as the Koopman operator approach, i.e.,

$$B_{kj} = \langle \hat{\varphi}_j, e^{t\mathcal{L}}\hat{\varphi}_k \rangle_{p_s} = \langle \hat{\varphi}_j, e^{t\hat{\mathcal{L}}}\hat{\varphi}_k \rangle_{p_s} = e^{\hat{\lambda}_k t} \delta_{jk}.$$

In DF method, the role of diffusion map is to estimate the eigenpairs of generator of gradient flow system (3.13). In this scenario, the diffusion map chooses an appropriate exponentially decaying function as the kernel  $k_\epsilon$  with bandwidth  $\epsilon$ , employs the kernel density estimate method to approximate the stationary density, and reconstruct a new kernel by removing the sampling bias from the stationary distribution. Then we apply a weighted graph Laplacian normalization to construct a transition kernel (or transition density)  $p_\epsilon$  corresponding to a Markov chain. The integral operator  $P_\epsilon$  is defined by

$$P_\epsilon f(x) := \int_{\mathcal{M}} p_\epsilon(x, y) f(y) p_s(y) dy.$$

Then its generator  $L_\epsilon f(x) := \frac{P_\epsilon f(x) - f(x)}{\epsilon}$  and converges to the infinitesimal generator of SDE (3.13), which is exactly what DF method seeks. Given a set of data points  $\{x_i\}_{i=1}^M$  sampled from the stationary distribution, the diffusion map algorithm furnishes the matrix approximation of the generator  $\hat{\mathcal{L}}$ , and the eigenpairs can be computed by SVD. In what follows, we describe DF and the diffusion map algorithm in Algorithm 2 and Algorithm 3, respectively.

---

**Algorithm 2** Diffusion forecast(DF)

---

**Input:** Time series  $\{x_i := x(t_i)\}_{i=1}^M \sim p_s(x)$ , the equilibrium measure  $p_s(x)$  and initial density function  $p_0(x)$ .

**Output:** The probability density function  $p(x, t)$ .

- 1: Compute the eigenpairs  $(\hat{\lambda}_i, \hat{\varphi}_i)$  of a specific operator  $\hat{\mathcal{L}}$ , also the generator of gradient flow (3.13) via diffusion maps algorithm outlined in Algorithm 3.
- 2: Estimate the probability density function  $p(x, t)$  by formula (3.14), (3.15) and (3.16) with  $\hat{c}_j(0) = \frac{1}{M} \sum_{i=1}^M p_0(x_i) \hat{\varphi}_i(x_i)$ .

---

REMARK 3.2. Through the comparison between our approach (DPDD) and diffusion forecast, we summarize the similarity and the difference between these two nonparametric methods. First of all, both of two methods require that the underlying system is ergodic and the given data sets are sampled from the unique invariant density function. One can ensemble the data from multiple trajectories, which can be realized by parallel simulation (or observation), rather than a single long-time trajectory. Secondly, for both approaches, the explicit expression of the invariant density is needed to fulfil an accurate estimation, while both can also work without knowing the invariant density through an appropriate method to approximate the density. Thirdly, for our approach, the orthonormal basis are the eigenfunctions of generator  $\mathcal{L}$  obtained from EDMD utilizing the relationship of Koopman operator  $\mathcal{K}$  and SDE generator  $\mathcal{L}$ , while the basis set for diffusion forecast method is the eigenfunctions of generator of a gradient flow system, computed by the diffusion map algorithm. Therefore, there exists approximation error when computing coefficients  $c_i(t)$  for the

diffusion forecast, while DPDD method analytically solves the coefficients. Finally, diffusion forecast is designed for autonomous dynamical systems, while DPDD can work for non-autonomous stochastic dynamical systems. For time-varying dynamical systems, the Koopman operator is dependent on time. Thus EDMD algorithm should be applied repeatedly for each temporal window where the dynamics is assumed to be autonomous.

---

**Algorithm 3** Diffusion Map Algorithm [6]

---

**Input:** Data  $\{x_i := x(t_i)\}_{i=1}^M$  sampled from the invariant density  $p_s(x)$  of gradient flow system.

**Output:** The approximate eigenpairs  $\{(\hat{\lambda}_i, v_i)\}$  of generator of gradient flow.

**1:** Choose a kernel  $k(x, y) = \exp(-\|x - y\|^2/2\epsilon^2)$  with an appropriate smoothing parameter called the bandwidth  $\epsilon$ .

**2:** Compute  $p_\epsilon(x) = \sum_j k(x, x_j)$ , renormalize and create the matrix  $\hat{K}$ , such that,

$$\hat{K}_{ij} = \frac{k(x_i, x_j)}{\sqrt{p_\epsilon(x_i)p_\epsilon(x_j)}}.$$

**3:** Define  $D_i = \sum_j \hat{K}_{ij}$  and construct a stochastic matrix  $P = D^{-1}\hat{K}$ , with entries

$$P_{ij} = \frac{\hat{K}_{ij}}{D_i}.$$

**4:** Define the generator matrix  $\hat{L} = \frac{P-I}{\epsilon}$ , and compute the first few eigenpairs of  $\hat{L}$ , s.t.,  $\hat{L}v = \hat{\lambda}v$ .

---

REMARK 3.3. We note that the integral operator  $P_\epsilon$  defined in the diffusion map algorithm is exactly the stochastic Koopman operator. Assuming that the invariant measure  $\nu$  is absolutely continuous with respect to the Lebesgue measure, and the Radon–Nikodym derivative is  $p_s(x)$ , we have,

$$\begin{aligned} P_\epsilon f(x) &= \int_{\mathcal{M}} p_\epsilon(x, y) f(y) p_s(y) dy \\ &= \int_{\mathcal{M}} p_\epsilon(x, y) f(y) d\nu \\ &= \mathbb{E}[f(\Phi(x))] \\ &= \mathcal{K}f(x), \end{aligned}$$

where  $\Phi(x) \sim p_\epsilon(x, \cdot)$  is the flow map of gradient flow system (3.13). Therefore, the diffusion map algorithm constructs the stochastic Koopman operator via a very different way from EDMD.

**4. Convergence Analysis.** When we use EDMD to approximate the probability density function of the stochastic dynamical system, the total error stems from three sources. One source of error, addressed in section 4.1, arises from the finite-dimensional approximation in EDMD, which is actually a Galerkin approximation of the Koopman operator [20, 37]. The convergence is achieved by sufficiently large number of data. The second source of error emerges when the spectral expansion is truncated at finite terms, and the number of truncated terms is equal to the dimensionality of observation space  $\mathcal{F}_D$ , which is spanned by the independent dictionary functions. This kind of error actually originates from the projection of Koopman operator onto the finite-dimensional subspace of the observables [21]. This error is addressed in section 4.2. Since the stochastic Koopman operator is defined as the expectation value of composition of observables and evolution operator, the data-driven

method should be implemented with the expectation of data pairs. However, the expectation of observables are usually elusive. Thus, when EDMD is applied to the stochastic system and the given data is the snapshot pairs of realized trajectories instead of expectations pairs, another source of error emerges. This kind of error will be briefly discussed in section 4.3. Finally, we give the weak convergence of the DPDD approximate probability density function to the analytic solution of Fokker-Planck equation.

**4.1. Convergence of EDMD to a Galerkin method.** Utilizing the Galerkin method, we obtain the matrices  $\hat{A}$  and  $\hat{G}$  whose entries

$$\begin{aligned}\hat{A}_{ij} &= \int_{\mathcal{M}} \psi_i(\Phi^{\Delta t}(x)) \psi_j(x) d\nu(x) = \langle \mathcal{K}\psi_i, \psi_j \rangle_{p_s}, \\ \hat{G}_{ij} &= \int_{\mathcal{M}} \psi_i(x) \psi_j(x) d\nu(x) = \langle \psi_i, \psi_j \rangle_{p_s},\end{aligned}\tag{4.1}$$

where  $\langle p, q \rangle_{p_s} = \int_{\mathcal{M}} p(x)q(x)p_s(x)dx$  is the inner product of the observable space. Then the finite-dimensional Galerkin approximation of Koopman operator would be  $\hat{K} = \hat{A}\hat{G}^{-1}$ .

Let the data points  $\{x_i\}_{i=1}^M$  be drawn from the invariant distribution  $\nu$  on  $\mathcal{M}$  with density  $\rho$  and the number of snapshots  $M \rightarrow \infty$ . We define the empirical measure  $\hat{\nu}_M$  by

$$\hat{\nu}_M = \frac{1}{M} \sum_{m=1}^M \delta_{x_m},\tag{4.2}$$

where  $\delta_{x_i}$  is the Dirac function at  $x_i$ . In particular, the  $ij$ -th elements of  $A$  and  $G$  are as follows,

$$\begin{aligned}A_{ij} &= \frac{1}{M} \sum_{m=1}^M \psi_i(y_m) \psi_j(x_m)^T = \int_{\mathcal{M}} \psi_i(\mathbf{F}(x)) \psi_j(x) d\hat{\nu}_M, \\ G_{ij} &= \frac{1}{M} \sum_{m=1}^M \psi_i(x_m) \psi_j(x_m)^T = \int_{\mathcal{M}} \psi_i(x) \psi_j(x) d\hat{\nu}_M.\end{aligned}\tag{4.3}$$

The  $ij$ -th elements of  $A$  and  $G$  contain the sample means of  $\psi_i(\mathbf{F}(x)) \psi_j(x)$  and  $\psi_i(x) \psi_j(x)$ . Thus, when  $M$  is finite, (4.1) is approximated by (4.3). By the law of large numbers, the sample mean almost surely converges to the expected value when the number of samples  $M$  is sufficiently large. Further, we have the following convergence with probability 1,

$$\lim_{M \rightarrow \infty} A_{ij} = \hat{A}_{ij}, \quad \lim_{M \rightarrow \infty} G_{ij} = \hat{G}_{ij}.\tag{4.4}$$

The convergence (4.4) could be read through two viewpoints. On the one hand, the convergence can be interpreted as the almost surely convergence of the empirical measure  $\hat{\nu}_M$  to the distribution  $\nu$  when there are sufficient data. On the other hand, we can consider the convergence as the result of the Monte-Carlo integration methods with independent identically distributed data. In this case, we have the convergence rate  $\mathcal{O}(M^{-1/2})$ .

**4.2. Convergence of the finite-dimensional subspace projection.** The convergence of EDMD to the Galerkin method has been discussed in Section 4.1. In computation, we use the finite-dimensional observable subspace projection  $\mathcal{K}_N$  of Koopman operator. Now we consider the convergence of the subspace operator  $\mathcal{K}_N$  to Koopman operator  $\mathcal{K}$ . This convergence was analyzed in [21]. Following the notation (3.3), we denote  $L^2(\mathcal{M}; p_s)$  norm of a function  $f$  by  $\|f\|_{0,p_s}$ . Given certain assumptions, the strong convergence of  $\mathcal{K}_N P_N^\nu$  to  $\mathcal{K}$  is addressed as follows.

**THEOREM 4.1.** [21] *Assume that Koopman operator  $\mathcal{K} : \mathcal{F} \rightarrow \mathcal{F}$  is bounded, and the observables  $\psi_1, \psi_2, \dots, \psi_N$  defining  $\mathcal{F}_D$  are selected from a given orthonormal basis of  $\mathcal{F}$ , i.e.,  $\{\psi_i\}_{i=1}^\infty$  is an orthonormal basis of  $\mathcal{F}$ . Then the sequence of operators  $\mathcal{K}_N P_N^\nu$  converges strongly to  $\mathcal{K}$  as  $N \rightarrow \infty$ , i.e.,*

$$\lim_{N \rightarrow \infty} \int_{\mathcal{M}} |\mathcal{K}_N P_N^\nu g - \mathcal{K}g|^2 d\nu = 0$$

for all  $g \in \mathcal{F}$ .

We note that  $P_N^\nu g$  is the  $L^2(\mathcal{M}; p_s)$ -projection of a function  $g \in \mathcal{F}$  onto  $\mathcal{F}_D$ . Besides, the weak convergence of the spectra of Koopman operator is given in the following theorem.

**THEOREM 4.2.** [21] *If  $\mu_N$  is a sequence of eigenvalues of  $\mathcal{K}_N$  with the associated normalized eigenfunctions  $\varphi_N \in \mathcal{F}_D$ , i.e.,  $\|\varphi_N\|_{0,p_s} = 1$ , then there exists a subsequence  $(\mu_{N_i}, \varphi_{N_i})$  such that*

$$\lim_{i \rightarrow \infty} \mu_{N_i} = \mu, \quad \varphi_{N_i} \xrightarrow{w} \varphi,$$

where  $(\mu, \varphi)$  is the eigenpair of Koopman operator such that  $\mathcal{K}\varphi = \mu\varphi$ .

**4.3. Convergence of the stochastic Koopman operator.** Now, we consider the stochastic system (2.1) in Section 2, and rewrite the model as

$$\frac{dX_t}{dt} = F(\eta_t, X_t), \quad (4.5)$$

where  $\eta_t$  is defined in form as the noise process  $\eta_t := \frac{dW_t}{dt}$ . Given the eigenpairs  $(\lambda, \varphi)$  of the generator  $\mathcal{L}$ , we have the following equation,

$$\frac{d\varphi}{dt} = \lambda\varphi + \tilde{F} \cdot \nabla\varphi, \quad (4.6)$$

where  $\tilde{F} = F - \mathbb{E}(F)$ . Similarly, when the model is written in the form of (2.1), we obtain the following equation [8],

$$d\varphi = \lambda\varphi dt + \nabla\varphi \sigma dW_t. \quad (4.7)$$

Thus, combining (4.6) and (4.7), we notice that  $\tilde{F} = F - \mathbb{E}(F) = \sigma \frac{dW_t}{dt} = \sigma\eta$ . From (2.12), for any observable  $g$ , we have  $\mathcal{K}^t g(x) = \mathbb{E}[g \circ \Phi^t(x)] = e^{t\mathcal{L}} g(x)$  and  $\mathcal{L}g(x) = \mathbb{E}(F) \cdot \nabla g$ . Thus a deviation arises when we use path data pairs instead of the expectation data pairs in EDMD for the approximation of stochastic Koopman

operator,

$$\begin{aligned}
g \circ \Phi^\tau - \mathcal{K}^\tau g &= g \circ \Phi^\tau - e^{\tau \mathcal{L}} g \\
&= e^{\tau \mathcal{L}_d} g - e^{\tau \mathcal{L}} g \\
&= (e^{\tau \mathcal{L}_d} - e^{\tau \mathcal{L}}) g \\
&\approx \mathcal{O}(\tau) \cdot (\mathcal{L}_d - \mathcal{L}) g \\
&= \mathcal{O}(\tau) \cdot (F - \mathbb{E}(F)) \cdot \nabla g \\
&= \mathcal{O}(\tau) \cdot \sigma \eta \cdot \nabla g,
\end{aligned} \tag{4.8}$$

where  $\mathcal{L}_d$  denotes the ‘‘deterministic generator’’ of (4.5), and satisfies  $\mathcal{L}_d g(x) = F \cdot \nabla g$ . For the approximate equality, we have used the first-order differentiation approximation of semigroups  $e^{\tau \mathcal{L}_d}$  and  $e^{\tau \mathcal{L}}$  around  $\tau = 0$  in accordance with the term-by-term differential properties in Prop. 2.2. The convergence of power series in [11] ensures that the linear approximation of Koopman operator in (4.8) converges to zero. Here we omit the proof for brevity. From (4.8), we note that the order of error  $\mathcal{O}(\tau)$  is achieved for the approximation of stochastic Koopman operator with EDMD using the snapshots pairs from stochastic systems. The time  $\tau$  is small enough so that the the first-order approximation of stochastic Koopman operator is accurate and tractable. This can be realized in the numerical simulation when the snapshot pairs are the state evolution with small temporal intervals.

**THEOREM 4.3.** *If the number of snapshots  $M$  and the dimension of finite-dimensional subspace projection  $N$  go to infinity, i.e.,  $M, N \rightarrow \infty$ , then the following convergence holds,*

$$A_{ij} \xrightarrow{a.s.} \hat{A}_{ij}, \quad G_{ij} \xrightarrow{a.s.} \hat{G}_{ij}, \quad \mathcal{K}_{M,N} \xrightarrow{a.s.} \mathcal{K}_N$$

and

$$\mathcal{K}_N \xrightarrow{\text{strongly}} \mathcal{K} \quad \text{in } L_2(\nu).$$

Thus, the approximation  $p_N(x, t)$  of the probability density function (3.6) weakly converges to  $p(x, t)$  in  $L^2(\mathcal{M}; p_s^{-1})$ , i.e.,

$$p_N(x, t) \xrightarrow{w} p(x, t), \quad \forall (x, t) \in \mathcal{M} \times \mathbb{R}^+, \tag{4.9}$$

where  $p_N(x, t) = \sum_{i=1}^N \tilde{c}_i(0) e^{\lambda_{N_i} t} \varphi_{N_i}(x) p_s(x)$  and  $(\lambda_{N_i}, \varphi_{N_i})$  are the eigenpairs in Theorem 4.2.

*Proof.* Combining the expression (3.6) of dynamic probability density decomposition and the approximation  $p_N(x, t)$ , we have

$$\begin{aligned}
p(x, t) - p_N(x, t) &= \sum_{i=1}^{\infty} c_i(0) e^{\lambda_i t} \varphi_i(x) p_s(x) - \sum_{i=1}^N \tilde{c}_i(0) e^{\lambda_{N_i} t} \varphi_{N_i}(x) p_s(x) \\
&= \sum_{i=1}^N e^{\lambda_{N_i} t} \varphi_{N_i}(x) p_s(x) (c_i(0) - \tilde{c}_i(0)) \\
&\quad + \sum_{i=1}^N (e^{\lambda_i t} \varphi_i(x) - e^{\lambda_{N_i} t} \varphi_{N_i}(x)) p_s(x) c_i(0) \\
&\quad + \sum_{i=N+1}^{\infty} e^{\lambda_i t} \varphi_i(x) p_s(x) c_i(0) \\
&\triangleq I + II + III.
\end{aligned} \tag{4.10}$$

Now, we analyze the three terms and show that all of them weakly converges to zero under the appropriate conditions. Firstly,  $\tilde{c}_i(0)$  is a Monte-Carlo integration approximation of coefficients  $c_i(0)$ , a strong convergence is ensured when  $M \rightarrow \infty$ . To address the second term  $II$ , we consider

$$e^{\lambda_i t} \varphi_i(x) - e^{\lambda_{N_i} t} \varphi_{N_i}(x) = e^{\lambda_i t} (\varphi_i(x) - \varphi_{N_i}(x)) + (e^{\lambda_i t} - e^{\lambda_{N_i} t}) \varphi_{N_i}(x).$$

By Theorem 4.2, we have the convergence of eigenvalues  $\lambda_{N_i} \rightarrow \lambda_i$  and the weak convergence of eigenfunctions  $\varphi_{N_i} \xrightarrow{w} \varphi_i$ . Therefore, the weak convergence of second term is also achieved.

As for the third term  $III$ , we recall that the eigenvalues of the generator  $\mathcal{L}$  is non-positive and descending sorted  $\lambda_0 = 0 > \lambda_1 > \lambda_2 > \dots$  with exponential decay, and as the eigenfunctions of FK operator,  $\varphi_i(x)p_s(x)$  can be considered as the smooth and bounded functions. In consequence, as dimensionality of observable space  $N$  goes towards infinity,  $e^{\lambda_i t}$  will decay rapidly to zero, so we conclude that the third term converges to zero. Therefore, the proof is completed.  $\square$

From the theorem above, we conclude that the spectral expansion of the probability density function will accurately approximate the truth density as the number  $M$  of data snapshots and the number  $N$  of observables are larger enough. The probability density can be used for the prediction of statistical moments, and provide the support to make decisions.

**5. Numerical results.** In this section, some numerical examples are given to illustrate the efficacy of the DPDD method and make the comparison for the two nonparametric forecast methods: Koopman operator forecast (DPDD) and diffusion forecast (DF). Subsection 5.1 is to show how the initial density function impacts on the approximation of DPDD approach. Subsection 5.2 demonstrates that if the underlying system is a gradient flow with isotropic diffusion, then the DPDD method agrees with the DF method. Both of them lead to an analytic expression for the coefficients  $c_i(t)$ . Subsection 5.3 and Subsection 5.4 show the comparison between DPDD and DF using a two-dimensional turbulence system and a noisy Lorenz-63 system, respectively. In Subsection 5.5, DPDD is used to forecast the ocean temperature, which is a realistic problem.

**5.1. The importance of the initial density condition.** As we have discussed in Section 3.2.2, the importance sampling is used to avoid sampling from the initial distribution. While the importance sampling method is more accurate when the alternative distribution  $p_s(x)$  is proportional to  $p_0(x)\varphi_i(x)$ . In this subsection, we will demonstrate that how the initial density  $p_0(x)$  affects the approximation of DPDD. For numerical simulation, we consider the following dynamical system,

$$dX_t = -4X_t(X_t - 1)(X_t + \frac{5}{4})dt + \sigma dW_t, \quad (5.1)$$

where  $\sigma$  is a constant. The corresponding deterministic dynamical system ( $\sigma = 0$ ) has two stable equilibrium points  $x = 1, -\frac{5}{4}$  and one unstable point  $x = 0$ . The stochastic system ( $\sigma = \sqrt{2}$ ) also has two potential pits, although the trajectories deviate from the stable equilibrium points under the random perturbations. The invariant distribution  $p_s(x)$  of the stochastic system,

$$p_s(x) = Z \exp \left\{ \frac{2}{\sigma^2} \int_0^x \left( -4u(u-1)(u+\frac{5}{4}) \right) du \right\} = Z \exp \left\{ -\frac{2}{\sigma^2} (x^4 + \frac{1}{3}x^3 - \frac{5}{2}x^2) \right\},$$

where  $Z = \int_{\mathcal{M}} \exp \left\{ \frac{2}{\sigma^2} \int_0^x (-4u(u-1)(u+\frac{5}{4})) du \right\} dx$  is the normalization constant. Figure 5.1 shows the stationary density, from which we can see that there are two equilibrium points with larger density and one unstable point with smaller density. The peaks of density function indicate that the stochastic state will trend to the stable points with large probability, while the valley shows that the state will escape from the unstable points.

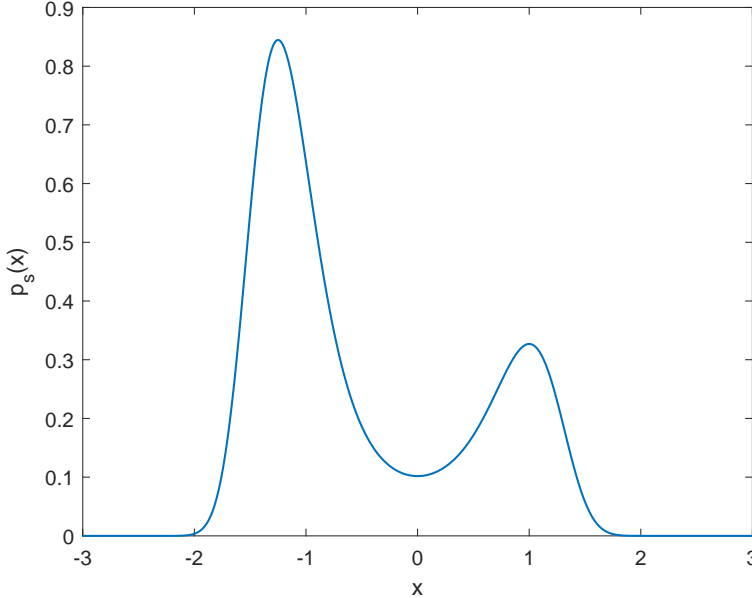


FIG. 5.1. *Stationary density function  $p_s(x)$*

We choose the polynomial functions  $\{x^n\}_{n=0}^5$  as the observation functions, sample  $M = 10000$  points from stationary density function  $p_s(x)$ , and utilize the snapshot data simulated by Euler-Maruyama scheme to compute the eigenpair  $(\lambda_i, \varphi_i(x))$  of Koopman operator  $\mathcal{K} = e^{t\mathcal{L}}$ , where  $\mathcal{L}$  is the infinitesimal generator of the stochastic system (5.1). Figure 5.2 shows the histogram of the samples, and Figure 5.3 depicts the empirical probability density function, which is acquired by a kernel density estimation method, a built-in algorithm *ksdensity.m* in Matlab. The true stationary density is used as reference.

Then we compute the probability density function as (3.12). One can forecast the density at any time. In this example, we directly solve the Fokker-Planck equation of dynamical system (5.1) as the reference solution. Firstly, let the initial density function  $p_0(x)$  be exactly the stationary density. The approximate probability density function by DPDD and the reference solution are depicted for six times in Figure 5.4, and the relative error is shown in Figure 5.5. From the above figures, we notice that the DPDD probability density tends to close to the reference solution, and the relative error deceases as the time advances. The DPDD solution quickly converges to the truth solution because the initial density is chosen to be the stationary density.

Another initial distribution  $x_0 \sim \mathcal{N}(0, 1)$  is selected for further comparison. The approximation solution and the relative error are showed in Figure 5.6 and Figure 5.7,

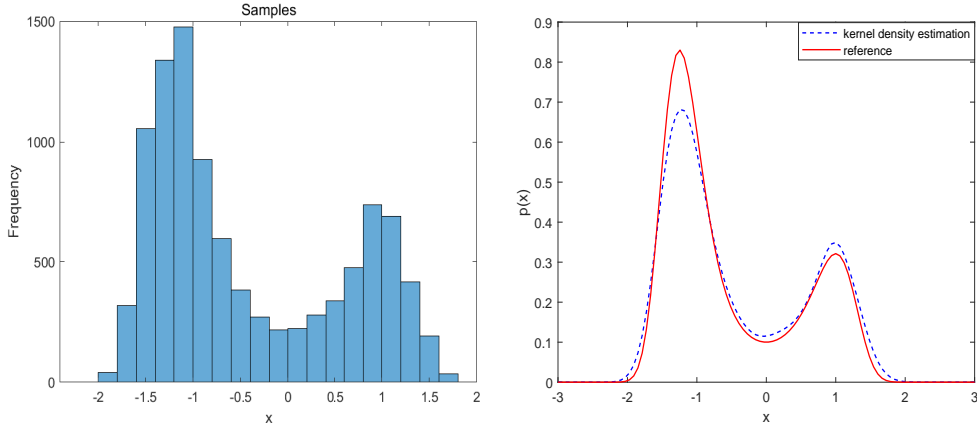
FIG. 5.2. Samples from  $p_s(x)$ 

FIG. 5.3. Empirical pdf of samples

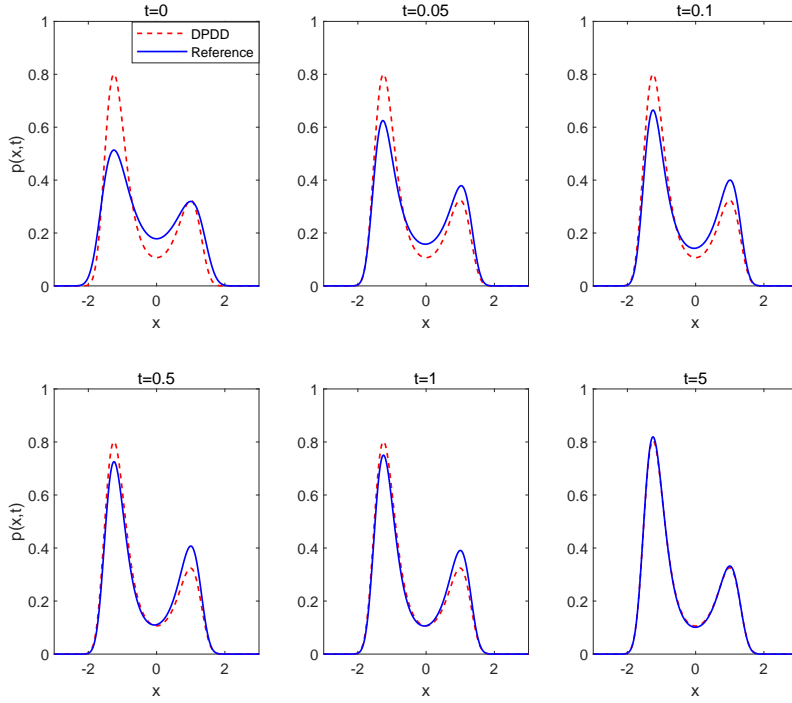
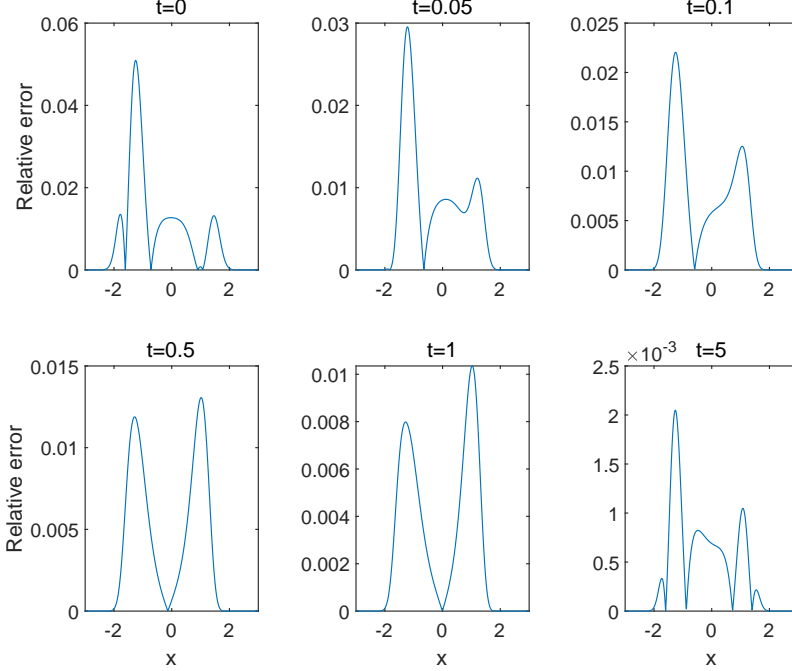


FIG. 5.4. The approximate pdf at different times.

respectively. In this case, the initial condition is very different from the stationary density, so the approximation is less accurate than the previous case, even though the estimation still becomes accurate as the time goes. Besides, Figure 5.5 and Figure 5.7 show that the approximation error in the both cases is larger at the peak and valley of the probability density function. This phenomena often occurs for multimodal model-

FIG. 5.5. *Relative error at different times.*

ing. The example confirms that if the initial density does not satisfy the proportional relation in the importance sampling approach, the variance of integration estimation may be large and lead to a significant DPDD approximation error. Therefore, the initial density impacts on the forecast accuracy.

**5.2. Ornstein Uhlenbeck process.** As we clarified in the previous Remark 3.1, the diffusion forecast (DF) method is consistent with our operator-theoretic approach DPDD when the underlying system is a gradient flow with isotropic diffusion. Therefore, in order to numerically illustrate the identity, we consider 1-dimensional OU process,

$$dX_t = -\lambda X_t dt + \beta dW_t, \quad X_0 = x_0. \quad (5.2)$$

Take the parameter  $\lambda = 1$ ,  $\beta = \sqrt{2}$ , thus the analytic expression of probability density function is given by

$$p(x, t) = \frac{1}{\sqrt{2\pi v^2(t)}} \exp\left(\frac{-(x - m(t))^2}{2v^2(t)}\right)$$

with mean  $m(t) = x_0 e^{-t}$  and variance  $v^2(t) = 1 - e^{-2t}$ , and the stationary states obey the standard normal distribution  $\mathcal{N}(0, 1)$ , i.e.,  $p_s(x) = \frac{1}{\sqrt{2\pi}} e^{-\frac{x^2}{2}}$ .

Moreover, the (infinitesimal) generator  $\mathcal{L} = -x \cdot \nabla + \Delta$ . Then the eigenvalues of generator of the OU process are the nonpositive integers  $\lambda_k = -k$ ,  $k = 0, 1, 2, \dots$ ,

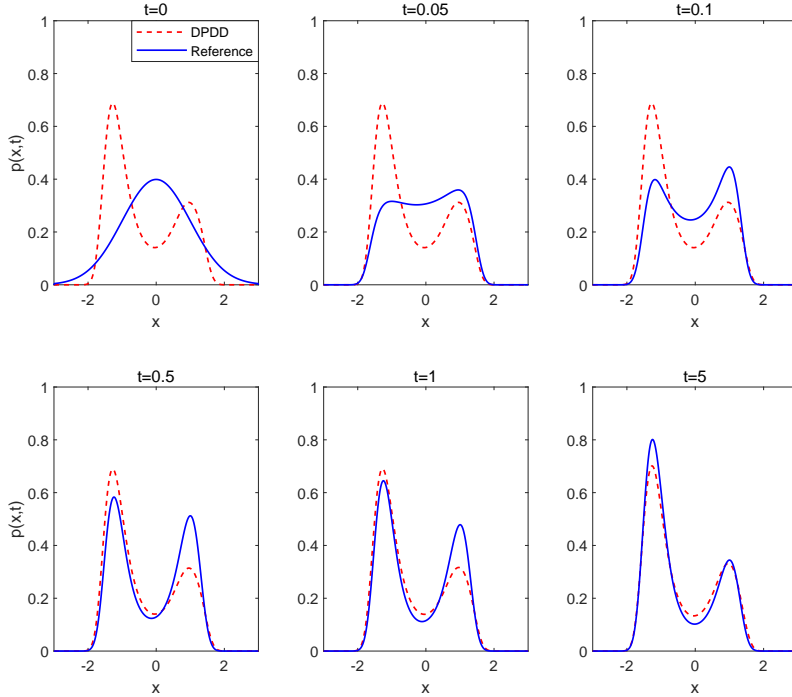


FIG. 5.6. The approximate pdf at different times.

and the corresponding eigenfunctions are the normalized Hermite polynomials

$$\varphi_k(x) = \frac{1}{\sqrt{k!}} H_k(x), \quad \text{with } H_k(x) = (-1)^k e^{\frac{x^2}{2}} \frac{d^k}{dx^k} (e^{-\frac{x^2}{2}}), \quad (5.3)$$

which form an orthonormal basis in  $L^2(\mathbb{R}; p_s)$ . In particular, the first three eigenfunctions are  $\varphi_0 = 1$ ,  $\varphi_1(x) = x$ ,  $\varphi_2(x) = \frac{1}{\sqrt{2}}(x^2 - 1)$ .

In this example, we simulate the OU process along a long time by Euler-Maruyama scheme and take 10001 states after a long-time enough evolution as the stationary samples. For the DPDD approach, we choose three monomial functions  $\{\psi_n(x) = x^n\}_{n=0}^2$  as observable functions. Thus the data matrices in (3.11) are two  $3 \times 10000$  matrices, satisfying the equation  $\Psi(Y) = \mathcal{K}\Psi(X)$ . For the diffusion forecast method, 10000 stationary samples are utilized, and three eigenfunctions are estimated by the diffusion map with variable bandwidth kernel.

In the following, we apply the two methods and show the eigenpairs, probability density functions and the first four moment functions to make a comparison. In Figure 5.8, we plot the analytic first three eigenfunctions listed in (5.3) as reference with the corresponding eigenvalues  $\lambda_0 = 0$ ,  $\lambda_1 = -1$ ,  $\lambda_2 = -2$ . The eigenfunctions approximated by two nonparametric methods are also illustrated in Figure 5.8. We notice that the both methods can estimate the first constant eigenfunction exactly, however the DF method is less accurate for approximation of the second and third eigenfunctions than DPDD. Besides, DPDD also has a better approximation for the corresponding eigenvalues than DF as illustrated in Table 5.1.

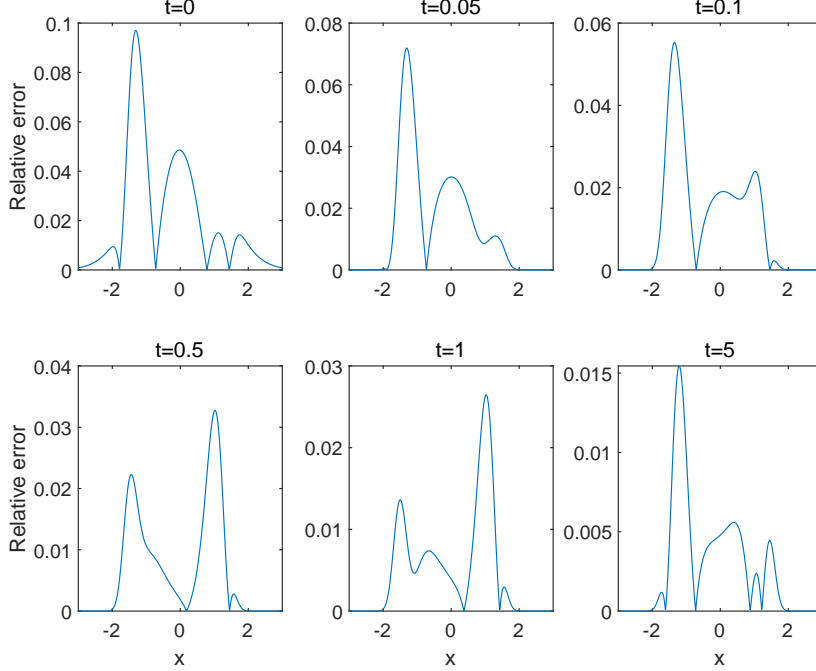
FIG. 5.7. *Relative error at different times.*

TABLE 5.1

*The first three eigenvalues estimated by DPDD and DF methods, with the analytic values as reference.*

Eigenvalues	$\lambda_0$	$\lambda_1$	$\lambda_2$
DF	$-1.1369 \times 10^{-13}$	-0.9163	-1.4233
DPDD	$2.2204 \times 10^{-14}$	-1.0052	-2.0974
Reference	0	-1	-2

To ensure the precision of importance sampling Monte-Carlo integration method, the initial condition is taken to be a Gaussian distribution whose mean is randomly picked from the stationary distribution and variance is 0.5. The behaviour of two approximate probability density functions at five different times is demonstrated in Figure 5.9, and the analytic solutions are given in the third column as reference. Figure 5.9 shows that, DPDD almost obtains the exact solution, while the DF method leads lots of deviations at many points. For the 1-dimensional OU process, the DPDD method gives a more accurate and robust approximation of the probability density function than the DF method.

Finally, we plot the evolutions of the first four-order raw moments in Figure 5.10 and the exact evolutions are directly computed by definition. From Figure 5.10, we observe that the both methods have a poor approximation at the beginning, since the initial condition is chosen very different from the true solution. Nevertheless, the approximations approach gradually to the truth evolution as the time goes. The moment functions given by DPDD are much closer to the analytic solutions and

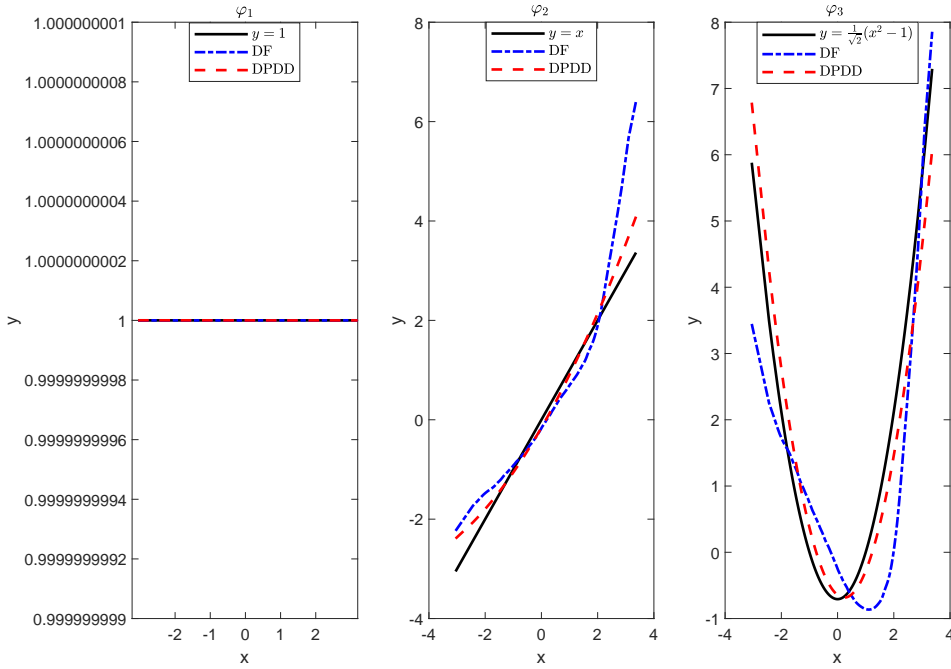


FIG. 5.8. The first three eigenfunctions estimated by DPDD and DF methods, and the analytic eigenfunctions (the normalized Hermite polynomials) are given in black.

converges quickly as time passes, while the DF method even does not converge to the truth for the two odd order moments. In summary, DPDD can better approximate the probability density and the moments than DF does. Thus better prediction is achieved through DPDD.

In the previous two examples, the dynamical systems, with additive noise, are 1-dimensional gradient flows with some potentials. Then we can easily solve the analytic solution of stationary density by directly computing the time-homogeneous Smoluchowski equation [27]. With the analytic density of stationary distribution, the spectral expansion (3.6) of the probability density in DPDD is more precise. However, the complex systems abound in the real world and there are often enormous challenges to simulate and characterize these systems. In what follows, we will consider the systems without knowing the truth stationary density, and estimate the steady-state density by the variable bandwidth kernel method [4]. We will still compare our approach with diffusion forecast method in the following numerical results. Since the analytic probability density is difficult to acquire, we will simulate plenty of trajectories of system states to get the sample data at any interested time, and use the corresponding point measure as reference, and this method is noted as an ensemble forecast [17]. The region where the sampling points are concentrated around corresponds to a large density, whereas the more sparse, the smaller the density.

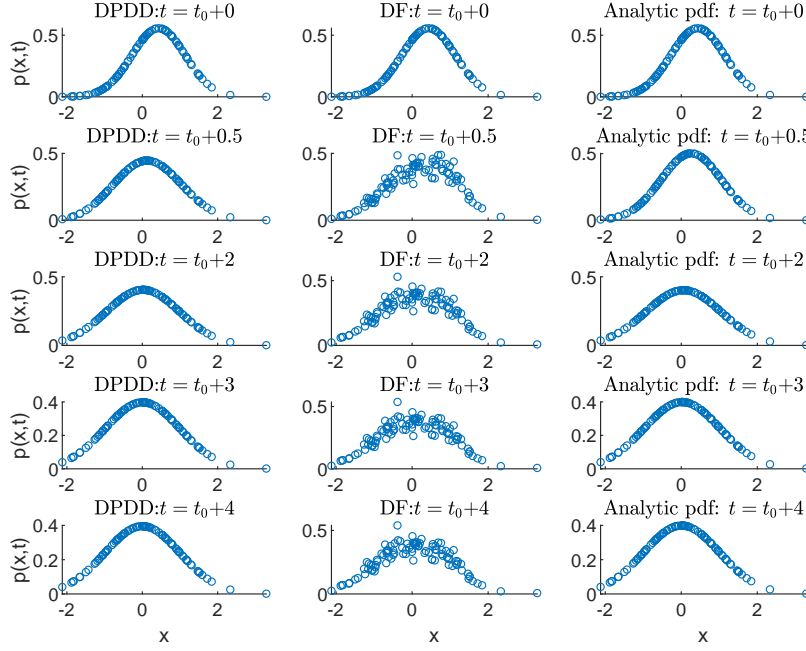


FIG. 5.9. The approximate probability density function given by DPDD and DF methods at different times, and the third column is the analytic solution.

**5.3. A quadratic turbulence system.** In this subsection, we consider the following two-dimensional system of SDE [17],

$$\begin{aligned} \frac{du}{dt} &= \frac{1}{2}uv - d\Lambda_{11}u + (1 - d\Lambda_{12})v + S_{11}\dot{W}_1 + S_{12}\dot{W}_2 \\ \frac{dv}{dt} &= -\frac{1}{2}u^2 + (-1 - d\Lambda_{12})u - d\Lambda_{22}v + S_{12}\dot{W}_1 + S_{22}\dot{W}_2, \end{aligned} \quad (5.4)$$

where the nonlinear terms conserve energy and  $\dot{W}_i$  denotes the independent white noise. This model is a special case of the paradigm model with persistently unstable dynamics for turbulence introduced in [33]. Here, we set the parameters in the model  $d = 1/2$ ,  $S = \Lambda^{1/2}$  with

$$\Lambda = \begin{pmatrix} 1 & 1/4 \\ 1/4 & 1 \end{pmatrix}.$$

Euler-Maruyama scheme is utilized to simulate the solutions of this model with time discretization  $\tau = 0.01$ . Using  $M = 20000$  snapshots data  $\{x_i = (u_i, v_i)\}_{i=1}^M$  and 4-dimensional observable  $\mathbf{g} = (1, u, v, (u + v)^2)^T$ , we approximate the stochastic Koopman operator, the Koopman eigenfunctions and eigenvalues by applying EDMD in the weighted space, and the eigenfunctions are evaluated at sample points. Once we obtain the eigenfunctions, we use them as the basis functions to get the spectral expansion of the probability density function as shown in Section 3. The number of truncation terms equals to the number of first few eigenfunctions, which is exactly the

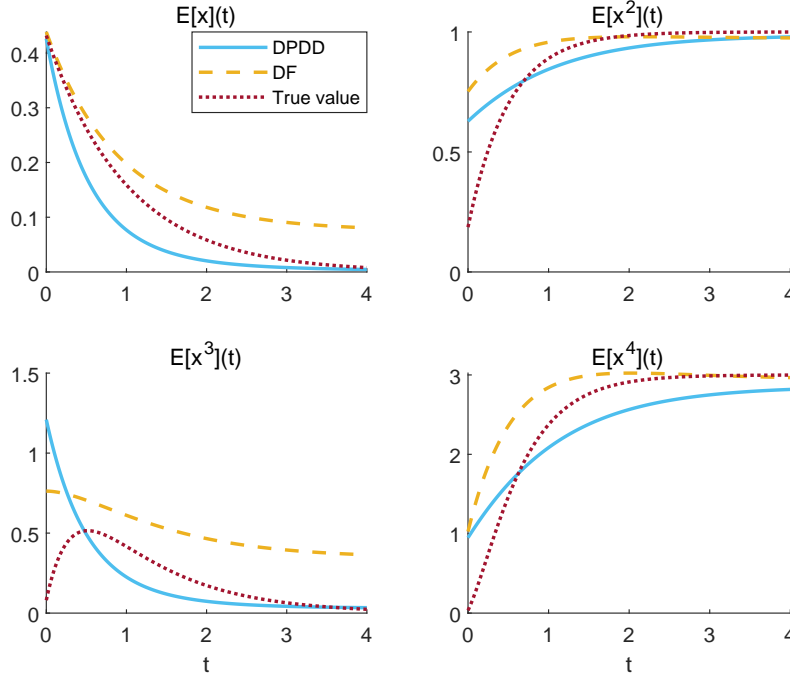


FIG. 5.10. The evolution of the first four-order raw moments estimated by DPDD (blue line) and DF (yellow dashed line) methods, and the reference is plotted in red dotted line.

dimensions of observable  $\mathbf{g}$ . The probability density function can be used to forecast and make a strategic decision.

As stated before, we compare our approach with the DF method, whose 1000 basis functions are constructed by diffusion maps algorithm, and an ensemble forecast is adopted as reference. In Figure 5.11, we plot the probability density function at five times  $t = 0, 0.5, 2, 3, 4$  obtained from different methods. In the first two columns of Figure 5.11, the color represents the value of density, and the yellow corresponds to larger value, while the blue is associated with smaller value. The region with dense points has large values of probability density in the last column. As we can see, the probability density functions approximated by two methods are very close to each other, and both match the distribution computed by ensemble forecast. The evolution of the first four raw moments of dynamical state are depicted as following.

From Figure 5.12, we find that as time goes, the both methods converge to almost the same value close to the reference. The obvious error exists because of the finite-dimensional truncation of the spectral expansion. For this example, we project the probability density function to a 4-dimensional space in DPDD approach, while DF method projects the density to a 1000-dimensional space. The average time to compute 1000 DF basis functions is about  $1.1 \times 10^3$  seconds, and the one to compute 4 DPDD basis functions is  $3.8 \times 10^{-3}$  seconds. A clear comparison is listed in Table 5.2, which shows that the DPDD method is much more computationally efficient than the DF method when they achieve a similar precision of approximation.

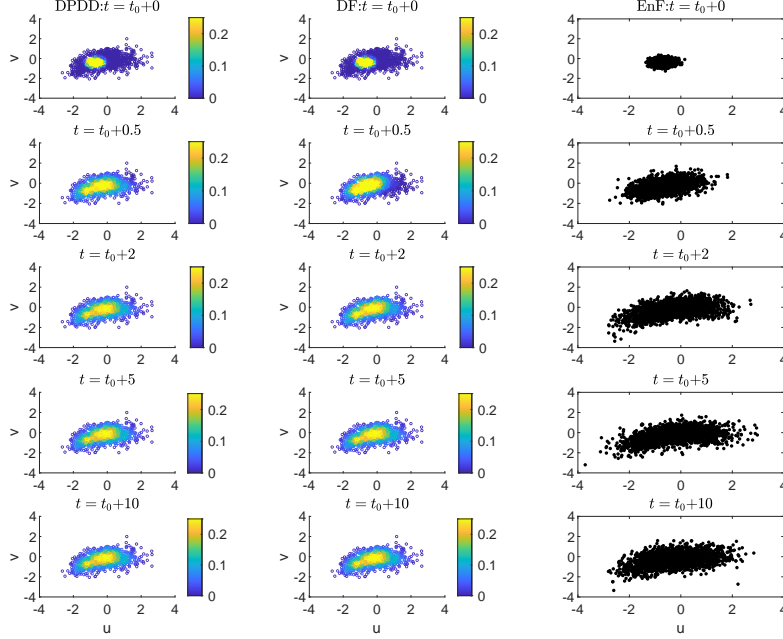


FIG. 5.11. The approximate probability density function at different times. The left column is estimated by DPDD, the middle is estimated by DF, and the right column (ensemble forecast) is given as reference.

TABLE 5.2  
The CPU time comparison of computing the corresponding eigenpairs

Method	DPDD	DF
The number of bases	4	1000
CPU time (s)	$3.8 \times 10^{-3}$	$1.1 \times 10^3$

**5.4. Noisy Lorenz-63 model.** In this subsection, we consider a more complex system - noisy Lorenz-63 model, which is intrinsically chaotic and stochastic. Noisy Lorenz-63 system characterizes the atmospheric convection model, and the governing equation is given by,

$$\begin{cases} \frac{dx}{dt} = \sigma(y - x) + q_x \eta_x \\ \frac{dy}{dt} = x(\rho - z) - y + q_y \eta_y \\ \frac{dz}{dt} = xy - \beta z + q_z \eta_z, \end{cases}$$

where the unknown functions  $x$ ,  $y$  and  $z$  represent the velocity, the horizontal temperature variation, and the vertical temperature variation, respectively. In the paper, we consider the system with standard Lorenz parameters Prandtl number  $\sigma = 10$ , the (relative) Rayleigh number  $\beta = 8/3$ , and the geometric factor  $\rho = 28$ . Besides, the stochastic force is assumed to be the independent Gaussian white noise with same

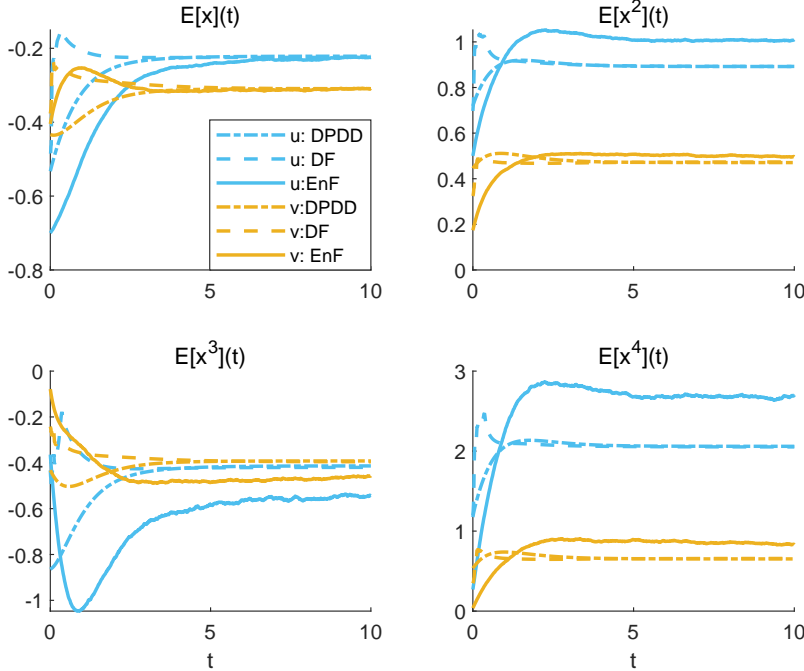


FIG. 5.12. The evolution of 1st-4th order raw moments of this two-dimensional system. The two dimensions are respectively depicted in “blue” and “yellow”. DPDD method corresponds to the dash-dotted line, DF method is corresponding to the dashed line, and the ensamble forecast, as reference, corresponds to the solid line.

intensity, i.e.,  $\eta_x dt, \eta_y dt, \eta_z dt \sim \mathcal{N}(0, dt)$  and  $q_x = q_y = q_z = 0.1$ . We simulate the trajectories in time interval  $[0, 100]$  by Runge-Kutta scheme with temporal step-size  $\Delta t = 0.01$ . We model the density by the DPDD method (with 2 basis functions) and the diffusion forecast (with 1000 basis functions), and the ensemble forecast solution is used for reference. A 3-dimensional scatter plot, where color of the circle corresponds to the value of density, is drawn in Figure 5.13. By Figure 5.13, we notice that the larger value of density is around the attractor. For a better visualization, we project the 3D scatter plot onto  $xOz$  plane. By Figure 5.13 and Figure 5.14, we find that the solution profile of DPDD is different from the solution profile of DF. This may be because of the strong instability of the chaotic system. The solution pattern by DPDD and DF looks similar to the ensemble forecast solution. For the simulation, DPDD uses 2 basis functions and DF uses 1000 basis functions. Thus, DPDD is more efficient than DF for any real-time computation.

**5.5. An ocean model.** In this subsection, we consider a more practical problem, the sea surface temperature (SST), which draws a vast interest in climate field. We have a global monthly SST dataset, the Extended Reconstructed Sea Surface Temperature (ERSST V5) [40] dataset, which includes the average monthly temperature from January 1854 to June 2022. The data set spatially covers the global (latitude: 88.0N - 88.0S, longitude: 0.0E - 358.0E), and is divided into an 89x180 grid. We take the 600 temporal data from January 1971 to December 2020 as observed data to estimate the eigenpairs, and the data from January 2020 to June 2022 as test data.

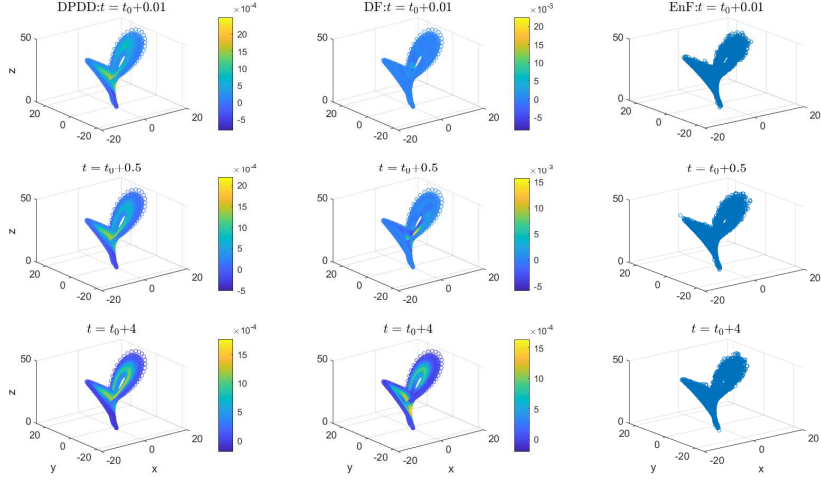


FIG. 5.13. The approximate probability density function obtained by different methods at different moments. Left(DPDD), middle(DF), right(EnF).

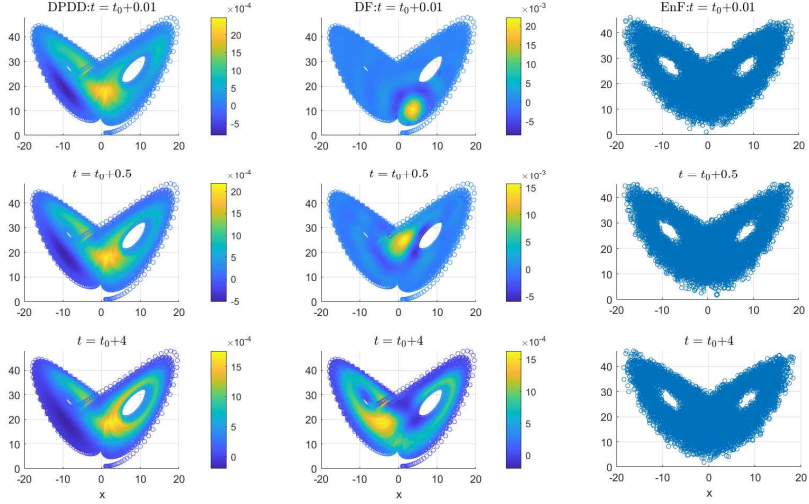


FIG. 5.14. The projected probability density function obtained by different methods at different moments. Left(DPDD), middle(DF), right(EnF).

Moreover, we will forecast the temperature for the second half year of 2022. The probability density functions for all the 16020 grid points are computed, which means that the total amount of data is  $9.612 \times 10^6$ .

The temperature figures at different months are presented to demonstrate the application of DPDD method solving the realistic problem. Figure 5.15 and Figure 5.16 show the approximate probability density functions of SST for different months in 2021 at two fixed locations, respectively. Comparing Figure 5.15 and Figure 5.16,

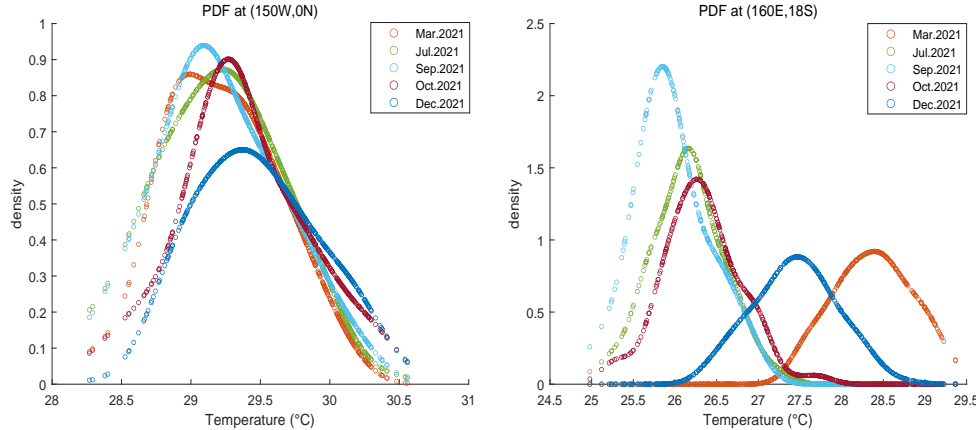


FIG. 5.15. *PDF of SST for five different months at 150 west longitude, 0 north latitude*

FIG. 5.16. *PDF of SST for five different months at 160 east longitude, 18 south latitude*

we find that the density function of average monthly temperature on the equator barely changes throughout the year, while the one in the southern hemisphere varies greatly. On the equator, higher temperatures are maintained all year with mean 29.2 centigrade degrees, and the maximum SST can be over 30 centigrade degrees. Whereas, in the southern hemisphere, temperatures are the highest for March (in summer) and lowest for September (in winter), which is the exact opposite of what happens in the northern hemisphere. The lowest SST can be 25 centigrade degrees in the southern hemisphere and the maximum rarely reaches 29.5 centigrade degrees, with a large temperature difference throughout the year. This indicates that the sea surface temperatures in southern and northern hemispheres are quite different from the equator. Then we approximate global SST for February 2020 and June 2021 comparing to true data, and also make a prediction for December 2022.

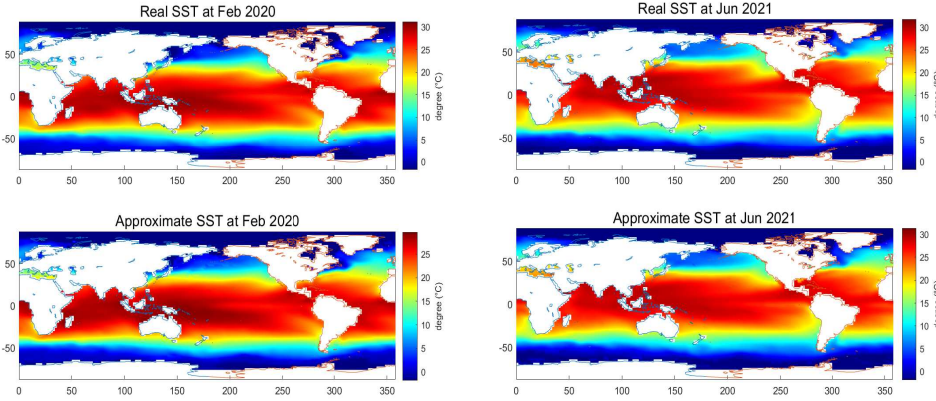


FIG. 5.17. *Global SST for February 2020, real data (top), approximate value (bottom).*

FIG. 5.18. *Global SST for September 2021, real data (top), approximate value (bottom).*

As depicted in Figure 5.17 and Figure 5.18, the approximate global SST is very

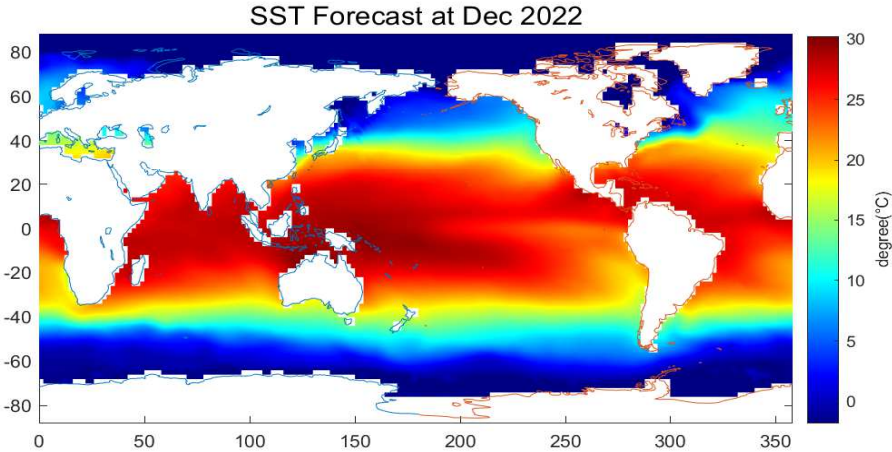


FIG. 5.19. *Global SST forecast for December 2022*

close to the reference value which is the real data from the dataset (ERSST v5). It is worth mentioning that the climate of the Mediterranean Sea in February is warm while it is torrid in June. In contrast, the sea surface temperature of the South Atlantic Ocean is higher in February than in June. And the prediction for December 2022 is illustrated in Figure 5.19. These figures show that the annual variation of SST in near-land areas is significantly larger than that in areas far from land, and the temperatures in southern and northern hemispheres change oppositely. DPDD sorts out this practical problem of having prodigious amounts of data, estimates the probability density functions well and predicts the state well, thus helps to make a scientific decision.

**6. Conclusion.** In this work, we have presented a nonparametric method, dynamic probability density decomposition (DPDD), to approximate the probability density functions for stochastic dynamical systems utilizing the data-driven mechanism. The snapshots of time-series data were sampled from the stationary distribution and can be one long-time trajectory or multiple trajectories. This approach was based on a stochastic Koopman formalism, operates on the snapshots, and estimated the probability density functions represented by the linear expansion of orthonormal basis functions in a weighted  $L^2$  space. This method has enabled us to represent the density functions as a finite-term truncation, and predicted the evolution of probability density for arbitrary time, and also the expectation values of observables. As a byproduct of DPDD, one can decompose arbitrary functions of dynamical state using the eigenfunctions of the infinitesimal generator of SDE, and the decomposition is similar to DPDD. Thus we can construct a dimensional reduction on data manifold. Comparing with diffusion forecast, DPDD behaviors better in applicability, model accuracy and computation efficiency. Moreover, we have given a rigorous convergence analysis of this method. Finally, DPDD was used to make probability density forecast for one-dimensional OU process, quadratic turbulence system, noisy-Lorenz-63, and a practical problem of global sea surface temperature.

- [1] H. ARBABI, I. MEZIĆ, *Ergodic Theory, Dynamic Mode Decomposition, and Computation of Spectral Properties of the Koopman Operator*, SIAM Journal on Applied Dynamical Systems, 16 (2017): 2096-2126.
- [2] T. BERRY, D. GIANNAKIS AND J. HARLIM, *Nonparametric Forecasting of Low-Dimensional Dynamical Systems*, Physical Review E, 91 (2015): 032915.
- [3] T. BERRY, J. HARLIM, *Nonparametric Uncertainty Quantification for Stochastic Gradient Flows*, SIAM/ASA Journal on Uncertainty Quantification, 3 (2015): 484-508.
- [4] T. BERRY, J. HARLIM, *Variable Bandwidth Diffusion Kernels*, Applied and Computational Harmonic Analysis, 40 (2016): 68–96.
- [5] S. L. BRUNTON, J. N. KUTZ, *Data-Driven Science and Engineering: Machine Learning, Dynamical Systems, and Control*, Cambridge: Cambridge University Press (2019).
- [6] R. R. COIFMAN, I. G. KEVREKIDIS, S. LAFON, ET AL., *Diffusion Maps, Reduction Coordinates, and Low Dimensional Representation of Stochastic Systems*, Multiscale Modeling & Simulation, 7 (2008): 842-864.
- [7] R. R. COIFMAN, S. LAFON, *Diffusion Maps*, Applied and Computational Harmonic Analysis, 21 (2006): 5-30.
- [8] N. ČRNJARIC-ŽIC, S. MAČEŠIĆ AND I. MEZIĆ, *Koopman Operator Spectrum for Random Dynamical Systems*, Journal of Nonlinear Science, 30 (2020): 2007–2056.
- [9] C. J. DSILVA, R. TALMON, C. W. GEAR, ET AL., *Data-Driven Reduction for a Class of Multiscale Fast-Slow Stochastic Dynamical Systems*, SIAM Journal on Applied Dynamical Systems, 15 (2016): 1327–1351.
- [10] N. B. ERICHSON, L. MATHELIN, J. N. KUTZ, ET AL., *Randomized Dynamic Mode Decomposition*, SIAM Journal on Applied Dynamical Systems, 18 (2019): 1867-1891.
- [11] K. J. ENGEL, R. NAGEL, *One-Parameter Semigroups for Linear Evolution Equations*, Graduate Texts in Mathematics, 194 (2000), Springer, New York.
- [12] G. FROYLAND, D. GIANNAKIS, B. R. LINTNER, ET AL., *Spectral Analysis of Climate Dynamics with Operator-Theoretic Approaches*, Nature Communications, 12 (2021): 6570.
- [13] C. W. GARDINER, *Handbook of Stochastic Methods-for Physics, Chemistry and the Natural Sciences*, Springer Series in Synergetics, 13 (1985), Springer-Verlag, Berlin, Heidelberg.
- [14] C. W. GARDINER, *Stochastic Methods-A Handbook for the Natural and Social Sciences*, Springer Series in Synergetics, 13 (2009), Springer-Verlag, Berlin, Heidelberg.
- [15] D. GIANNAKIS, *Data-Driven Spectral Decomposition and Forecasting of Ergodic Dynamical Systems*, Applied and Computational Harmonic Analysis, 47 (2019): 338-396.
- [16] M. S. GUTIÉRREZ, V. LUCARINI, M. D. CHEKROUN, ET AL., *Reduced-Order Models for Coupled Dynamical Systems: Data-Driven Methods and the Koopman Operator*, Chaos: An Interdisciplinary Journal of Nonlinear Science, 31 (2021): 053116.
- [17] J. HARLIM, *Data-Driven Computational Methods: Parameter and Operator Estimations*, Cambridge: Cambridge University Press (2018).
- [18] L. JIANG, N. LIU, *Correcting Noisy Dynamic Mode Decomposition With Kalman Filters*, Journal of Computational Physics, 461 (2022): 111175.
- [19] B. O. KOOPMAN, *Hamiltonian Systems and Transformation in Hilbert Space*, Proceedings of the National Academy of Sciences, 17 (1931): 315-318.
- [20] S. KLUS, P. KOLTAI AND C. SCHÜTTE, *On the Numerical Approximation of the Perron-Frobenius and Koopman Operator*, Journal of Computational Dynamics, 3 (2016): 51-79.
- [21] M. KORDA, I. MEZIĆ, *On Convergence of Extended Dynamic Mode Decomposition to the Koopman Operator*, Journal of Nonlinear Science, 28 (2018): 687–710.
- [22] B. O. KOOPMAN, J. v. NEUMANN, *Dynamical Systems of Continuous Spectra*, Proceedings of the National Academy of Sciences, 18 (1932): 255-263.
- [23] M. LI, L. JIANG, *Deep Learning Nonlinear Multiscale Dynamic Problems Using Koopman Operator*, Journal of Computational Physics, 446 (2021): 110660.
- [24] I. MEZIĆ, *Spectral Properties of Dynamical Systems, Model Reduction and Decompositions*, Nonlinear Dynamics, 41 (2005): 309–325.
- [25] B. ØKSENDAL, *Stochastic Differential Equations: An Introduction with Applications-Fifth Edition*, Universitext (2003), Springer-Verlag, Berlin, Heidelberg .
- [26] A. PAZY, *Semigroups of Linear Operators and Applications to Partial Differential Equations*, Applied Mathematical Sciences, 44 (1983), Springer-Verlag, New York.
- [27] G. A. PAVLIOTIS, *Stochastic Processes and Applications: Diffusion Processes, the Fokker-Planck and Langevin Equations*, Texts in Applied Mathematics, 60 (2014), Springer, New York.
- [28] G. A. PAVLIOTIS, A. M. STUART, *Multiscale Methods: Averaging and Homogenization*, Texts in Applied Mathematics, 53 (2008), Springer-Verlag, New York.
- [29] D. RUELLE, *Statistical Mechanics of a One-dimensional Lattice Gas*, Communications in Math-

ematical Physics, 9 (1968): 267–278.

[30] C. W. ROWLEY, I. MEZIĆ, S. BAGHERI, ET AL., *Spectral Analysis of Nonlinear Flows*, Journal of Fluid Mechanics, 641 (2009): 115–127.

[31] S. SINHA, B. HUANG AND U. VAIDYA, *On Robust Computation of Koopman Operator and Prediction in Random Dynamical Systems*, Journal of Nonlinear Science, 30 (2020): 2057–2090.

[32] P. J. SCHMID, *Dynamic Mode Decomposition of Numerical and Experimental Data*, Journal of Fluid Mechanics, 656 (2010): 5–28.

[33] T. P. SAPSIS, A. J. MAJDA, *Blending Modified Gaussian Closure and Non-Gaussian Reduced Subspace Methods for Turbulent Dynamical Systems*, Journal of Nonlinear Science, 23 (2013): 1039–1071.

[34] S. SÄRKÄÄ, A. SOLIN, *Applied Stochastic Differential Equations (Institute of Mathematical Statistics Textbooks)*, Cambridge: Cambridge University Press (2019).

[35] N. TAKEISHI, Y. KAWAHARA AND T. YAIRI, *Subspace Dynamic Mode Decomposition for Stochastic Koopman Analysis*, Physical Review E, 96 (2017): 033310.

[36] J. H. TU, C. W. ROWLEY, D. M. LUCHTENBURG, ET AL., *On Dynamic Mode Decomposition: Theory and Applications*, Journal of Computational Dynamics, 1 (2014): 391–421.

[37] M. O. WILLIAMS, I. G. KEVREKIDIS AND C. W. ROWLEY, *A Data-Driven Approximation of the Koopman Operator: Extending Dynamic Mode Decomposition*, Journal of Nonlinear Science, 25 (2015): 1307–1346.

[38] M. O. WILLIAMS, C. W. ROWLEY AND I. G. KEVREKIDIS, *A Kernel-Based Method for Data-Driven Koopman Spectral Analysis*, Journal of Computational Dynamics, 2 (2015): 247–265.

[39] F. ZANINI, A. CHIUSO, *Estimating Koopman Operators for Nonlinear Dynamical Systems: a Nonparametric Approach*, IFAC-PapersOnLine, 54 (2021): 691–696.

[40] NOAA NATIONAL CENTERS FOR ENVIRONMENTAL INFORMATION, *NOAA Extended Reconstructed SST V5*, NOAA PSL, Boulder, Colorado, USA, <https://psl.noaa.gov>.